AMERICAN SOCIETY FOR MICROBIOLOGY | Molecular and Cellular Biology®

RESEARCH ARTICLE

Critical Role of Matrix Metalloproteinase 14 in Adipose Tissue Remodeling during Obesity

Xin Li,[a] Yueshui Zhao,[a]* Chuan Chen,[b] Li Yang,[a] Hyun-ho Lee,[a] Zening Wang,[b] Ningyan Zhang,[c] Mikhail G. Kolonin,[a] Zhiqiang An,[c] Xin Ge,[b] Philipp E. Scherer,[d] Kai Sun[a]

[a]Center for Metabolic and Degenerative Diseases, The Brown Foundation Institute of Molecular Medicine for the Prevention of Human Diseases, University of Texas Health Science Center at Houston, Houston, Texas, USA

[b]Department of Chemical and Environmental Engineering, University of California, Riverside, California, USA

[c]Texas Therapeutics Institute, The Brown Foundation Institute of Molecular Medicine for the Prevention of Human Diseases, University of Texas Health Science Center at Houston, Houston, Texas, USA

[d]Touchstone Diabetes Center, UT Southwestern Medical Center at Dallas, Dallas, Texas, USA

ABSTRACT Fibrosis is recognized as the major pathological change in adipose tissue during the development of obesity. However, the detailed mechanisms governing the interactions between the fibrotic components and their modifiers remain largely unclear. Here, we reported that matrix metalloproteinase 14 (MMP14), a key pericellular collagenase, is dramatically upregulated in obese adipose tissue. We generated a doxycycline-inducible adipose tissue-specific MMP14 overexpression model to study its regulatory function. We found that overexpression of MMP14 in the established obese adipose tissue leads to enlarged adipocytes and increased body weights in transgenic mice. Furthermore, the mice exhibited decreased energy expenditure, impaired lipid metabolism, and insulin resistance. Mechanistically, we found that MMP14 digests collagen 6α3 to produce endotrophin, a potent costimulator of fibrosis and inflammation. Unexpectedly, when overexpressing MMP14 in the early-stage obese adipose tissue, the transgenic mice showed a healthier metabolic profile, including ameliorated fibrosis and inflammation, as well as improved lipid and glucose metabolism. This unique metabolic phenotype is likely due to digestion/modification of the dense adipose tissue extracellular matrix by MMP14, thereby releasing the mechanical stress to allow for its healthy expansion. Understanding these dichotomous impacts of MMP14 provides novel insights into strategies to treat obesity-related metabolic disorders.

KEYWORDS adipose tissue, collagen 6, ECM, HIF1, MMP14, obesity, endotrophin, fibrosis, inflammation, lipid metabolism

Obesity has become a worldwide threat to public health. It has been associated with many other chronic metabolic diseases, such as cardiovascular diseases (CVD), type 2 diabetes, and certain types of cancer (1). Over the past few decades, the central role of adipose tissue in the development of obesity-associated metabolic dysfunction has been recognized (2–4). As such, it is widely accepted that dysfunctional adipose tissue *per se* can lead to systemic insulin resistance and other metabolic disorders (2).

However, not all adipose tissue expansion is necessarily associated with pathological changes (1). The concept of a "metabolically healthy obese" state suggests that "healthy" adipose tissue bypasses the pathological steps and thus preserves systemic insulin sensitivity. To illustrate this, we recently reported that vascular endothelial growth factor A (VEGF-A)-induced stimulation of angiogenesis in adipose tissues improves vascularization and exerts protective effects against high-fat-diet-mediated metabolic insults (5). Intriguingly, we and others further demonstrated that the con-

Citation Li X, Zhao Y, Chen C, Yang L, Lee H-H, Wang Z, Zhang N, Kolonin MG, An Z, Ge X, Scherer PE, Sun K. 2020. Critical role of matrix metalloproteinase 14 in adipose tissue remodeling during obesity. Mol Cell Biol 40:e00564-19. https://doi.org/10.1128/MCB.00564-19.

Copyright © 2020 American Society for Microbiology. All Rights Reserved.

Address correspondence to Kai Sun, kai.sun@uth.tmc.edu.

* Present address: Yueshui Zhao, Laboratory of Molecular Pharmacology, Department of Pharmacology, School of Pharmacy, Southwest Medical University, Luzhou, Sichuan, China.

Received 7 November 2019
Returned for modification 1 December 2019
Accepted 22 January 2020
Accepted manuscript posted online 27 January 2020
Published 30 March 2020

sequences of modulation of angiogenic activity are dichotomous and context dependent: proangiogenic activity during adipose tissue expansion at early stage of obesity development is beneficial, whereas the same action in the context of "unhealthy" expansion in the established obese adipose tissue leads to metabolic dysfunction (5–9). In addition to VEGF-A, we hypothesize there may be other players involved in the regulation in adipose tissues that exert dichotomous effects on the expanding fat mass.

A key step during the progression of adipose tissue from the lean to the obese state is the development of hypoxia due to the inability of vascular bed to keep pace with the rapid tissue expansion (10–13). Hypoxic adipose tissue has unique alterations that contribute to its dysfunction. Among them, fibrosis is a key feature of metabolic dysfunction in the tissue (1, 14, 15). Emerging evidence supports the notion that fibrosis is a major player in adipose tissue dysfunction by decreasing extracellular matrix (ECM) flexibility (15–21). Of note, abnormal collagen accumulation during ECM remodeling is tightly associated with local inflammation in adipose tissue, which further leads to systemic insulin resistance (21–25). Furthermore, proinflammatory factors and elevated levels of free fatty acids produced by unhealthy adipose tissue further trigger an elevated degree of lipotoxicity in other organs, such as the liver, the heart, and muscle (26–29). Importantly, the fibrotic reaction in obese adipose tissue is efficiently prevented by inhibition of hypoxia inducible factor 1α (HIF1α) using pharmacological and genetic approaches. This also highlights that this pathological process can be reversed (14).

Excessive collagen deposition is synonymous with fibrosis in adipose tissue (18). Among all the collagen family members, collagen 6 (COL6) is the most abundant microfilaments in adipose tissue (19, 30, 31). As a large collagenous glycoprotein, COL6 is composed of three chains: α1, α2, and α3. These three chains are assembled into heterotetramers and secreted into the extracellular space, where they further associate to form mature microfibrils (20). During the development of diet-induced obesity, COL6 is excessively deposited into the ECM. This stiff and inflexible matrix constitutes a physical barrier against further adipose tissue expansion. The ensuing mechanical stress ultimately leads to local and systemic metabolic dysregulation (10, 18). To illustrate this further, mice lacking COL6 exhibit destabilized ECM and hence display reduced fibrosis in adipose tissue (19). Interestingly, despite exhibiting overall larger adipocytes and larger fat mass, the COL6 knockout mice on a high-fat diet (HFD) or with an *ob/ob* background are metabolically healthier with improved insulin sensitivity (19).

The three chains (α1, α2, and α3) of COL6 are synthesized in the cytosol and form oligomers with each other and are deposited into the extracellular compartment to form ECM (19). Importantly, we recently discovered that the carboxy-terminal C5 domain of the α3 chain is proteolytically cleaved from the parental COL6 microfibrils during the secretion process (20, 32, 33). The product of this cleavage step, named endotrophin, is stable and has been found to be enriched not only in obese adipose tissue but also in the circulation and urine of the patients with certain heart or kidney conditions (34–36). Moreover, endotrophin is found at higher levels in human breast cancer specimens (20, 30). As a newly identified small molecule with potent bioactivity, the adverse effects of endotrophin in different tissues have been extensively studied. Previously, we reported that endotrophin stimulates fibrosis and inflammation within the preexisting obese adipose tissue. As a result, obese mice exhibit systemic insulin resistance (37). Blocking endotrophin with a neutralizing antibody significantly ameliorates the metabolically adverse effects and reverses metabolic dysfunction caused by HFD (37). Importantly, we discovered that endotrophin serves as a potent mediator to promote malignant tumor progression (20). In the tumor tissue, endotrophin increases fibrosis, angiogenesis and is a proinflammatory player via activating transforming growth factor β (TGF-β) signaling (20). Most recently, a clinical study revealed that circulating endotrophin is correlated with heart failure (34). Two other observations indicate that urinary endotrophin is associated with development of end-stage renal diseases and serum endotrophin levels correlate with increased mortality in chronic kidney disease (35, 36). Collectively, these studies highlight endotrophin as a potential

target from a therapeutic perspective in the context of metabolism and cancer (38–40). However, the detailed mechanisms governing endotrophin's biogenesis and the collagenase(s) responsible for cleavage remain unclear.

Matrix metalloproteinases (MMPs) are a large family of endopeptidases that digest ECM proteins in both physiological and pathological conditions (41, 42). There are 23 MMPs in human tissues, and they are divided into soluble-type MMPs and membrane-bound-type MMPs (MT-MMPs) (43–45). While soluble-type MMPs are secreted and diffused directly into the ECM, MT-MMPs are tethered to the plasma membrane and exert their enzymatic function(s) at the cell surface (46). Among the family of MMPs, MMP14, also known as MT-MMP1, is the predominant pericellular collagenase in adipose tissue (47). Its mRNA levels are upregulated during obesity, along with many other MMPs (48). Loss-of-function of MMP14 leads to impaired adipose tissue formation, eventually leading to severe lipodystrophy in mice (49). A genetic variant in the human MMP14 gene has been found to be linked to obesity and diabetes (50). Together, these findings demonstrate a key role of MMP14 in physiological/pathological remodeling of adipose tissue. The regulation profile of its collagenase activity and its specific substrates in adipose tissue remain poorly defined (47).

In this study, we reported that MMP14 protein levels increase in both early- and late-stage obese adipose tissue, and HIF1α is the transcriptional factor that modulates its upregulation. Importantly, we identified COL6α3 as the substrate for MMP14. We generated a doxycycline (Dox)-inducible adipose tissue-specific MMP14 overexpression model to study its role in adipose tissue remodeling during obesity. We found that when overexpressed, MMP14 in the preexisting (established) obese adipose tissue digests COL6α3 within its C5 domain. MMP14 thereby produces endotrophin, which in turn stimulates fibrosis and leads to macrophage accumulation in adipose tissue. As a result, the transgenic mice exhibit adverse metabolic consequences. This includes impaired glucose and lipid metabolism, decreased energy expenditure, and systemic insulin resistance. Interestingly, when MMP14 is overexpressed in early-stage obese adipose tissue, it prevents abnormal accumulation of fibrotic proteins and hence promotes healthy expansion of fat pads. Our study thus suggests that MMP14 plays an important but dichotomous role for adipose tissue expansion.

RESULTS

MMP14 is upregulated in adipose tissue of mice during different stages of obesity. To investigate how the endogenous MMP14 in adipose tissue is regulated during obesity, we challenged wild-type C57/BL6J mice with HFD for 5 and 18 weeks and measured the MMP14 levels. The Western blotting result showed that MMP14 protein level is increased in epididymal white adipose tissues (eWAT) during HFD feeding (Fig. 1A; quantitative measurement of Western blotting in Fig. 1B). Furthermore, Col6α level is also increased (Fig. 1A and B). The quantitative PCR (Q-PCR) results further revealed that the mRNA level of Mmp14 and Col6α are upregulated in eWAT upon HFD feeding (Fig. 1C). To rule out the effect of ageing during the study, we compared the levels of MMP14 at the same time points upon HFD feeding. The Q-PCR results showed that Mmp14 mRNA is upregulated in eWAT upon HFD feeding (Fig. 1D). The Western blotting result further revealed that MMP1 protein level is also increased (Fig. 1E; quantitative measurement in Fig. 1F). We then measured MMP14 levels after long-term HFD feeding for 18 weeks. We found that both the expression level and the protein level are increased in the eWAT (Fig. 1G and H; quantitative measurement of Western blotting in Fig. 1I). Interestingly, the upregulation of Mmp14 is also observed in eWAT of the genetically obese mice (*ob/ob* mice) (Fig. 1J), suggesting that obesity itself, independent of whether it is induced by HFD or genetic factors, is sufficient to lead to an elevation of MMP14 in adipose tissue.

MMP14 is upregulated by HIF1α in obese adipose tissue. Given that hypoxia is the initial pathological change during the development of obesity (1), we next determined whether hypoxia inducible factor 1α (HIF1α) is involved in the regulation of MMP14. Q-PCR analysis revealed that treatment with PX-478, a selective HIF1α inhibitor

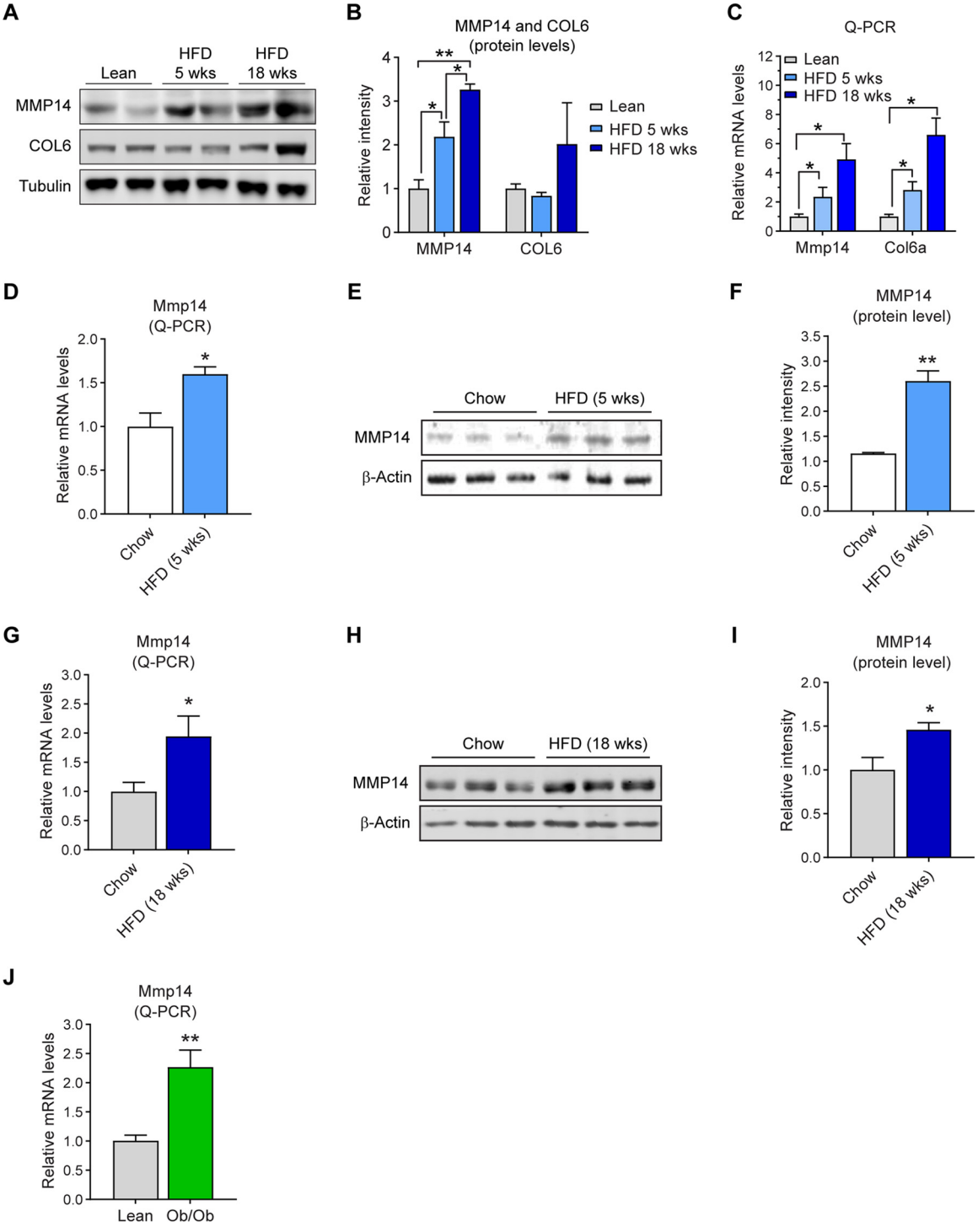

FIG 1 MMP14 is upregulated in adipose tissue of mice during different stages of obesity. (A) Western blotting of MMP14 and COL6 in the eWAT of wild-type (WT) lean, 5-week, and 18-week HFD-fed mice ($n = 4$ per group, representative of three trials). (B) Quantification of the band density for the Western blotting in panel A ($n = 4$ per group, one-way ANOVA; *, $P < 0.05$; **, $P < 0.01$). (C) Q-PCR analysis of Mmp14 and Col6a genes in the eWAT of WT lean, 5-week, and 18-week HFD-fed mice ($n = 4$ per group, one-way ANOVA; *, $P < 0.05$). (D) Q-PCR analysis of Mmp14 gene in the eWAT of WT mice that were fed on regular chow diet or HFD for 5 weeks ($n = 5$ per group, Student *t* test; *, $P < 0.05$). (E) Western blotting of MMP14 in the eWAT of WT mice that were fed regular chow diet or HFD for 5 weeks ($n = 5$ per group, representative of three trials). (F) Quantification of the band density for the Western blotting in panel E ($n = 5$ per group, Student *t* test; **, $P < 0.01$). (G) Q-PCR analysis of *Mmp14* genes in the eWAT of WT mice that were fed on regular chow diet or HFD for 18 weeks ($n = 6$ per group, Student *t* test; *, $P < 0.05$). (H) Western blotting of MMP14 in the eWAT of WT mice that were fed on regular chow diet or HFD for 18 weeks ($n = 6$ per group, representative of three trials). (I) Quantification of the band density for the Western blotting in panel H ($n = 6$ per group, Student *t* test; *, $P < 0.05$). (J) Q-PCR analysis of the *Mmp14* genes in the eWAT of *ob/ob* and their littermate lean control mice ($n = 6$ per group, Student *t* test; **, $P < 0.01$).

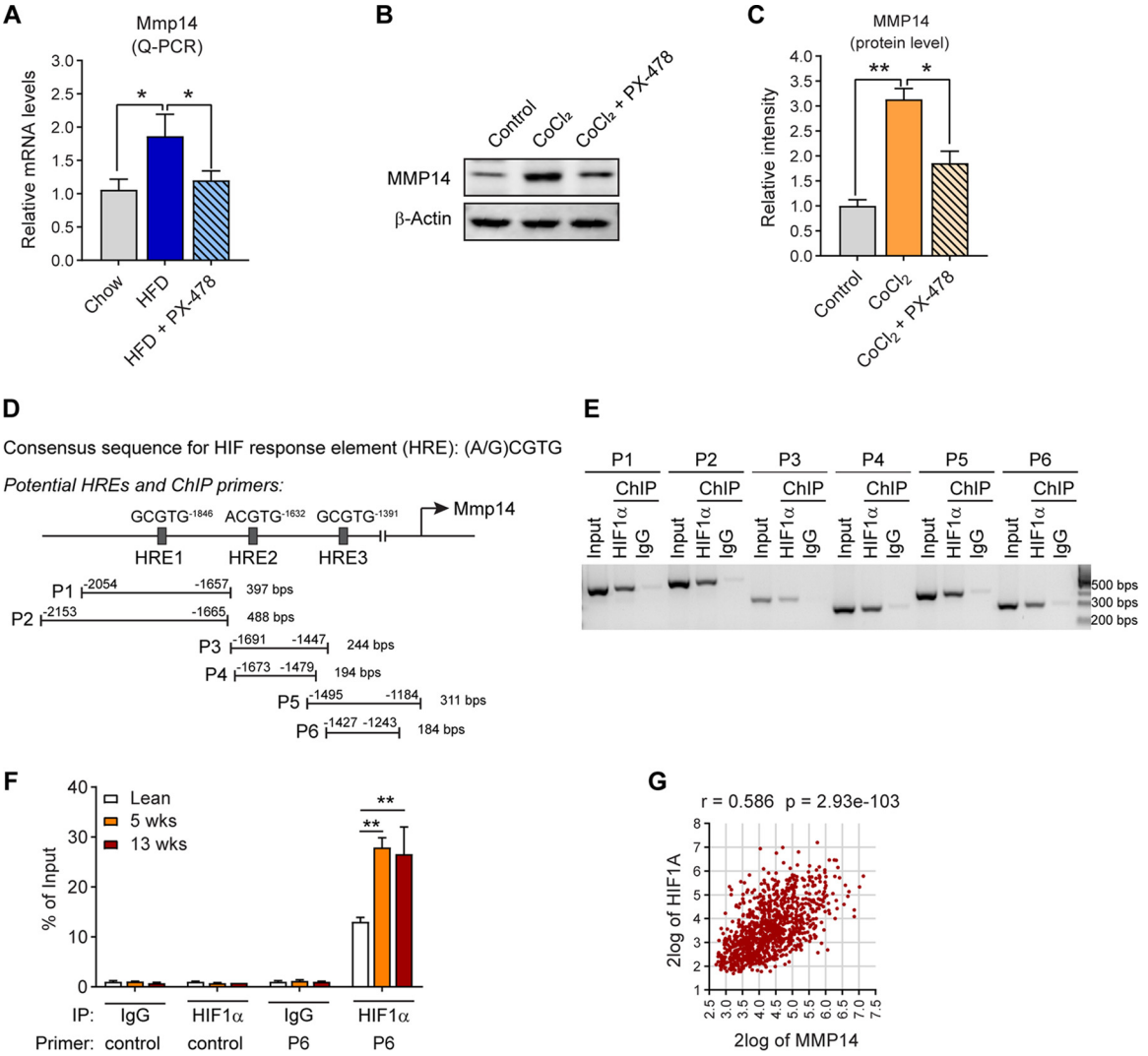

FIG 2 MMP14 is upregulated by HIF1α in obese adipose tissue. (A) Q-PCR analysis of *Mmp14* in the eWAT of WT mice that were fed on regular chow diet, HFD, or HFD plus PX-478 (HIF1α inhibitor) for 5 weeks ($n = 5$ per group, one-way ANOVA; *, $P < 0.05$). (B) Western blotting of MMP14 in PC3 cells treated with $CoCl_2$ (100 μM) in the presence or absence of PX-478 (30 μM; representative of three trials). (C) Quantification of the band density for the Western blotting in panel B ($n = 3$ per group, one-way ANOVA; *, $P < 0.05$; **, $P < 0.01$). (D) Schematic diagram showing the three potential HIF response elements (HREs) in the 2,000 bp upstream sequence of the mouse *Mmp14* gene. Six pairs of ChIP primers were designed to probe the different regions containing the potential HREs. The sizes of predicted products of ChIP-PCR assay are indicated at the end of each primer. (E) Semiquantitative PCR analysis of ChIP assay in hypoxia PC3 cells using the primers indicated in panel D and the DNA templates immunoprecipitated by anti-HIF1α antibody or IgG (negative control). (F) Q- PCR analysis of ChIP assay in the eWAT of lean, 5-week, and 18-week HFD-fed mice. The Q-PCR analysis was performed against the DNA templates immunoprecipitated by anti-HIF1α antibody or IgG with the control and P6 primers as indicated in panel D. The data are presented as the percentages of immunoprecipitation input for each sample (representative of three trials, $n = 3$ per group, one-way ANOVA; **, $P < 0.01$). (G) Correlation analysis between MMP14 and HIF1A genes in the public breast tumor data set ($n = 1110$) using genomics analysis and the visualization platform R2. The correlation coefficient *r* value and the significance *P* value were autocalculated by the platform.

(14, 51–53) suppresses the upregulation of Mmp14 induced by HFD (Fig. 2A). Moreover, MMP14 protein level increases upon $CoCl_2$ treatment, a condition that mimics the effects of hypoxia. Parallel treatment with PX-478 during $CoCl_2$ exposure significantly suppresses the MMP14 level (Fig. 2B; quantitative measurement in Fig. 2C). Together, the results clearly suggest that HIF1α is involved in MMP14 regulation. Notably, when searching the promoter region of Mmp14, we identified at least three sequences that match the consensus motif for HIF1α response element (HRE; A/GCGTG) (Fig. 2D, top diagram). To test whether HIF1α binds to these HREs, we performed a chromatin immunoprecipitation (ChIP) assay with an anti-HIF1α antibody. The primers that rec-

ognize the HREs in the Mmp14 promoter region and the sizes of the products were indicated (Fig. 2D, bottom diagram). The results revealed that HIF1α binds to all the HREs with high affinity (Fig. 2E). To determine whether the bindings are regulated by HFD feeding, we performed a quantitative ChIP assay with P6 and the tissue lysates from the eWAT of HFD-fed mice. The Q-PCR results revealed more HIF1α bind to P6 upon HFD feeding for 5 and 13 weeks, while no bindings were detected by the control primer (Fig. 2F). Our results demonstrate that HIF1α binds to Mmp14 promoter and regulates its expression in response to HFD feeding.

Tumor-surrounded WAT has been revealed to be involved in breast cancer progression. Once the cancer cells become intermingled with adipocytes and other cells of WAT, a cross talk ensues (54). Hypoxia induced ECM-associated factors have been demonstrated to play an important role in breast cancer initiation and promotion (20). We then sought to determine the correlation between HIF1α and MMP14 in tumor samples of the breast cancer patients performing a Pearson correlation analysis on a large data set of patients with breast cancer (https://hgserver1.amc.nl/cgi-bin/r2/main.cgi). Interestingly, we found a correlation between HIF1A and MMP14 ($n = 1110$; $r = 0.586$, $P < 0.001$) (Fig. 2G).

Inducible overexpression of MMP14 in established obese adipose tissue leads to increased body weight, larger adipose tissues, and fatty liver. To study the physiological/pathological function of MMP14 in adipose tissue, we generated a doxycycline (Dox)-inducible adipocyte-specific MMP14 overexpression mouse model. We bred the adiponectin-rtTA (Apn-rtTA) mice with tetracycline response element (TRE)-driven MMP14 transgenic mice to generate the transgenic line (Apn-rtTA-TRE-Mmp14). Offspring from the crossed mouse strains overexpresses titratable amounts of MMP14 in response to different doses of Dox. Of note, the TRE-Mmp14 mice also constitutively overexpress tTS, which binds to TRE to prevent any potential for leaky expression. Upon Dox treatment, rtTA efficiently replaces tTS to activate the overexpression of Mmp14 (Fig. 3A). By taking advantage of this transgenic model, we were able to study MMP14 in a physiological setting during different stages of obesity. To characterize the inducible overexpression, the transgenic mice, along with their littermate controls, were fed with regular chow diet containing 200 mg/kg Dox for 1 week, and then the overexpression levels of MMP14 in different tissues were detected. The level of transgene Mmp14 was detected with a real-PCR primer that specifically recognizes Mmp14-Flag transcripted from the TRE plasmid. The results showed that the overexpression of Mmp14 was significantly induced in adipose tissues, especially in eWAT but not in other tissues, such as the liver in the transgenic mice. No overexpression was detected in the wild-type controls (WT) (Fig. 3B). Moreover, no overexpression was detected without Dox induction (Fig. 3B). We further confirmed the increased protein levels of MMP14 (Fig. 3C; quantification in Fig. 3D) and increased mRNA levels of pan MMP14 in eWAT (Fig. 3E). Of note, we manipulated the protein levels of MMP14 well within the physiological range, leading up to a doubling of the levels. One week of induction of MMP14 in adipose tissue under regular chow did not change the body weights of the transgenic mice compared to the littermate controls (Fig. 3F). This argues that we had successfully established a triple transgenic mouse model for the investigation of MMP14 in obese adipose tissue.

To study the function of MMP14 in preexisting (established) obese adipose tissue, we fed the 6-week-old transgenic mice and their littermate controls using a HFD for 13 weeks to induce obesity. Then, the mice were fed by HFD plus 200 mg/kg Dox for 5 more weeks (Fig. 3G). The results revealed that the transgenic mice dramatically gain more body weights (Fig. 3H and I). The change is mostly caused by the increased fat mass (Fig. 3J), while the lean mass shows no difference (Fig. 3K). Measurements of the tissue samples further confirmed that the fat pads, including the eWAT, subcutaneous white adipose tissue (sWAT), brown adipose tissues (BAT), are larger in the transgenic mice (Fig. 3L). Furthermore, hematoxylin and eosin (H&E) staining revealed that the eWAT and BAT exhibit larger adipocytes and that the liver accumulates significantly more lipid (Fig. 3M). Quantitative measurements further revealed that the size of the

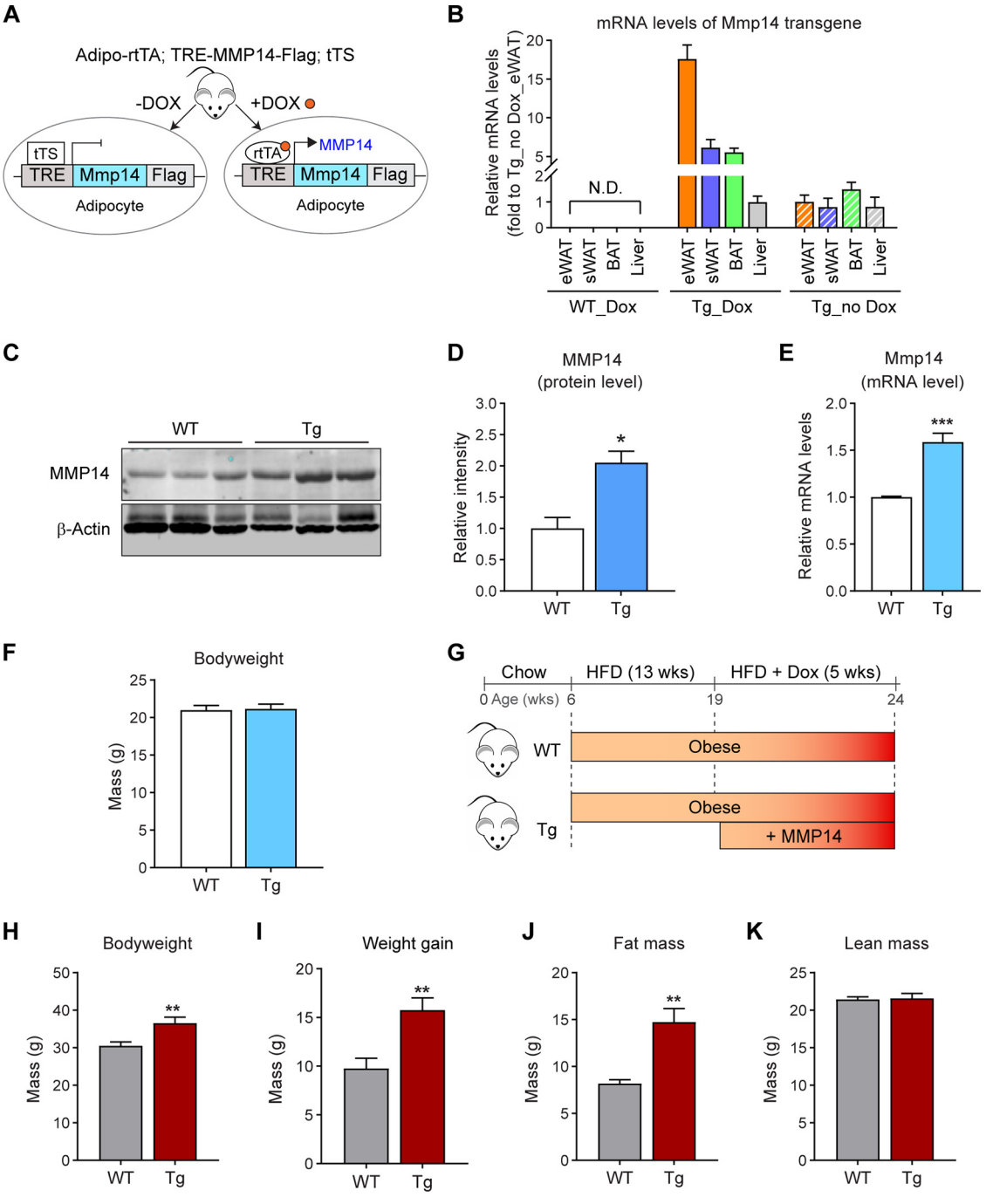

FIG 3 (Continued)

adipocytes in the eWAT is significantly larger in the transgenic mice, while the average size of adipocytes is similar in sWAT (Fig. 3N to Q). Collectively, overexpression of MMP14 in established obese adipose tissues leads to larger adipose tissue and fatty liver in the transgenic mice. Moreover, it leads to an increased lipogenesis, which is in agreement with the previous study (50).

Overexpression of MMP14 in established obese adipose tissue causes impaired energy expenditure. Obese mice frequently exhibit lower energy expenditure. Intriguingly, metabolic cage studies indicated that MMP14-overexpressing mice in the background of previously established obesity consume even less oxygen and produce less carbon dioxide during both light and dark cycles compared to their littermate controls

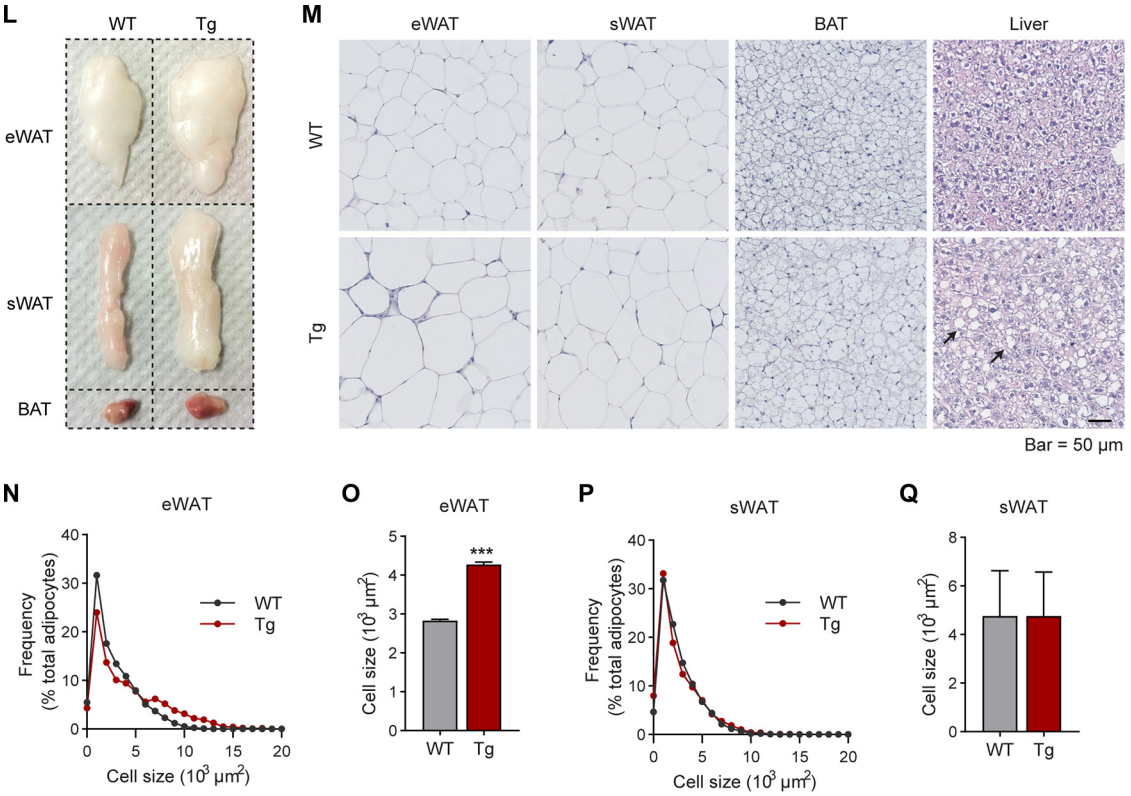

FIG 3 Inducible overexpression of MMP14 in established obese adipose tissue leads to increased body weight, larger adipose tissue, and fatty liver. (A) Newly generated mouse model for Dox-inducible adipocyte-specific overexpression of MMP14. Mice carrying triple transgenes (Adipo-rtTA; TRE-Mmp14-flag; tTS) were used as MMP14 Tg mice, while their littermates carrying Adipo-rtTA only were used as WT controls. (B) Q-PCR analysis of the *Mmp14* transgene in different tissues of MMP14 Tg and WT mice that were fed with or without doxycycline (Dox; 200 mg/kg regular chow diet) for 1 week. The primer pair for the Q-PCR analysis specifically recognized the transgenic *Mmp14* but not endogenous *Mmp14* by probing the Flag tag at the 3′ end of transgenic *Mmp14* ($n = 3$ per group). (C) Western blotting of MMP14 in the eWAT of MMP14 Tg and WT mice fed on Dox (200 mg/kg regular chow diet) for 1 week ($n = 6$ per group, representative of three trials). (D) Quantification of the band density for the Western blotting in panel C ($n = 6$ per group, Student *t* test; *, $P < 0.05$). (E) Q-PCR analysis of the *Mmp14* gene in the eWAT of MMP14 Tg and WT mice that were fed with or without Dox (200 mg/kg regular chow diet) for 1 week. The primer pair for Q-PCR recognized both the transgenic and endogenous *Mmp14* by probing the exons of *Mmp14* ($n = 6$ per group, Student *t* test; ***, $P < 0.001$). (F) Body weights of MMP14 Tg and WT mice upon Dox (200 mg/kg regular chow diet) feeding for 1 week ($n = 6$ per group, Student *t* test). (G) Schematic diagram showing the long-term HFD feeding program. The MMP14 Tg and WT mice were fed on HFD for 13 weeks and then fed on HFD plus DOX (200 mg/kg diet) for 5 more weeks. (H) Body weights of MMP14 Tg and WT mice after a long-term HFD feeding as shown in panel G ($n = 5$ or 6 per group, Student *t* test; **, $P < 0.01$). (I) Gains in body weight of MMP14 Tg and WT mice after a long-term HFD feeding ($n = 5$ or 6 per group, Student *t* test; **, $P < 0.01$). (J) MRI analysis for fat mass of MMP14 Tg and WT mice after a long-term HFD feeding ($n = 5$ or 6 per group, Student *t* test; **, $P < 0.01$). (K) MRI analysis for lean masses of MMP14 Tg and WT mice after a long-term HFD feeding ($n = 5$ or 6 per group, Student *t* test). (L) Images of eWAT, sWAT, and BAT collected from MMP14 Tg and WT mice after a long-term HFD feeding. (M) H&E staining of eWAT, sWAT, BAT, and liver collected from MMP14 Tg and WT mice after long-term HFD feeding. The arrows indicate lipid droplets accumulated in the liver. (N) Frequency distribution of different-sized adipocytes of eWAT of MMP14 Tg and WT mice after long-term HFD feeding (adipocytes from five to six mice per group were analyzed). (O) Comparison of average adipocyte sizes of eWAT between MMP14 Tg and WT mice after long-term HFD feeding (adipocytes from five to six mice per group were analyzed, Student *t* test; ***, $P < 0.001$). (P) Frequency distribution of different-sized adipocytes of sWAT in MMP14 Tg and WT mice after long-term HFD feeding (adipocytes from five to six mice per group were analyzed). (Q) Comparison of average adipocyte sizes of sWAT between MMP14 Tg and WT mice after long-term HFD feeding (adipocytes from five to six mice per group were analyzed, Student *t* test).

(Fig. 4A to D). Furthermore, the transgenic mice produced less heat while the respiratory exchange rate (RER) did not show a difference from the controls (Fig. 4E to H). Of note, the transgenic mice did not show differences in food intake and activity (Fig. 4I and J). Together, when overexpressing MMP14 in established obese adipose tissue, the transgenic mice exhibit impaired energy expenditure under HFD.

Overexpression of MMP14 in established obese adipose tissue leads to abnormal glucose and lipid metabolism in the transgenic mice. Adipose tissue pathological changes have been linked directly to adverse metabolic profiles systemically. We therefore tested glucose metabolism in the MMP14 transgenic mice and their littermate

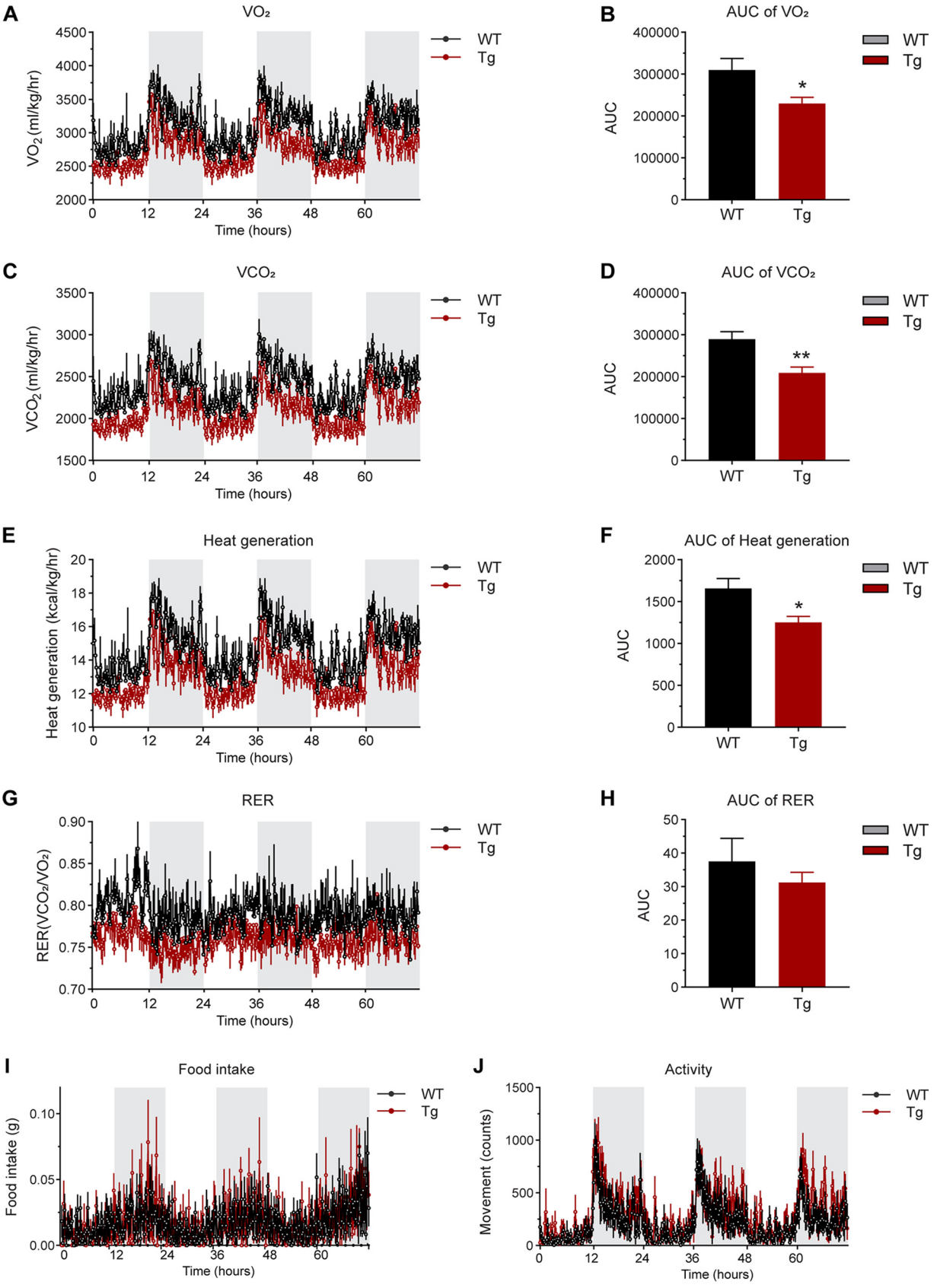

FIG 4 Overexpression of MMP14 in established obese adipose tissue causes impaired energy expenditure. (A) O_2 consumption profile of MMP14 Tg and WT mice in a 12-h light-dark cycle after long-term HFD feeding ($n = 5$ or 6 per group). (B) The area under the curve (AUC) of O_2

(Continued on next page)

controls. An intraperitoneal glucose tolerance test (IPGTT) revealed that the transgenic mice are less glucose tolerant than the controls (Fig. 5A; quantification of the curve areas is shown in Fig. 5B). In line with the IPGTT result, the fasting circulating insulin level showed a trend toward an increase in the transgenic mice (Fig. 5C). Furthermore, the phospho-AKT level is decreased in the eWAT and sWAT of MMP14 transgenic mice, while the total level does not show any significant changes (Fig. 5D and F). The quantitative measurements of the ratio of phospho-ATK to total AKT further confirm the blunted AKT phosphorylation (Fig. 5E and G). Similar changes were also detected in liver (Fig. 5H and I). Given that MMP14 has been reported to modulate stromal vascular fraction differentiation through a mechanism independent of proteolysis which hence affects adipogenesis and lipogenesis (50), we then analyzed the profile for lipid metabolism. The profile shows that the circulating levels for triglycerides are increased in the transgenic mice (Fig. 5J). Moreover, the circulating levels of glycerol and nonesterified free fatty acids (FFA) also show trends toward an increase in the transgenic mice (Fig. 5K and L). The triglycerides in liver are also increased in the transgenic mice (Fig. 5M). Consistent with these observations, the lipogenesis genes, including *Accl*, *Fasn*, and *Plin1*, are all upregulated in the eWAT of transgenic mice (Fig. 5N). Combined, the results suggest that the overexpression of MMP14 in established obese adipose tissue leads to both local and systemic dysregulation of glucose and lipid metabolism.

Overexpression of MMP14 in established obese adipose tissue stimulates local fibrosis and inflammation. The major function of MMP14 is to digest collagens for ECM remodeling. We thus investigated ECM-related genes in the adipose tissue of the transgenic mice. The Q-PCR results reveal that a series of collagen genes, including *Col1a1*, *Col2a1*, *Col3a1*, and *Col6a3*, as well as *Fibronectin*, are upregulated in the eWAT of the transgenic mice (Fig. 6A). Western blotting analysis further conformed the increased protein level of COL6 (Fig. 6B; quantitative measurements in Fig. 6C). Moreover, the gene for collagen-modifying enzyme *Lox* (lysyl oxidase) (55) is also upregulated
(Fig. 6D). Interestingly, other members of MMPs, such as *MMP2* and *MMP12*, are upregulated, reflecting a positive feedback of MMP14 overexpression (Fig. 6E). Importantly, the TGF-β receptor 1 gene (*Tgfβr1* is also upregulated (Fig. 6F). In agreement with the upregulation of fibrotic genes, trichrome staining revealed that the level of fibrosis in eWAT of the transgenic mice is enhanced (Fig. 6G; indicated by dark blue). Quantitative measurement of the blue signals by ImageJ further confirmed the result (Fig. 6H). Importantly, the gene correlation analyses on the public genomic data set (https://hgserver1.amc.nl/cgi-bin/r2/main.cgi) demonstrated that the level of MMP14 has tight correlation to COLs, fibronectin (FN), and TGF-β1 (Fig. 6I to P).

Fibrosis is highly associated with local inflammation in adipose tissue (18). We thus examined the local inflammation in the transgenic mice. Q-PCR results revealed that key proinflammatory genes, including *Tnfα* and *F4/80*, are upregulated, while the anti-inflammatory gene *Il10* was downregulated in the eWAT of transgenic mice (Fig. 6Q). Interestingly, the M1-macrophage marker *Cd86* is upregulated (Fig. 6R), while the M2-macrophage marker, *Cd163* is downregulated (Fig. 6S), reflecting a proinflammatory microenvironment in the eWAT of the transgenic mice. Furthermore, Mac2 (marker of macrophage) staining revealed that the "crown-like" structures (CLS), which reflect

FIG 4 Legend (Continued)
consumption in 12-h light and 12-h dark time after a long-term HFD feeding ($n = 5$ or 6 per group; *, $P < 0.05$). (C) CO_2 production profile of MMP14 Tg and WT mice in a 12-h light-dark cycle after long-term HFD feeding ($n = 5$ or 6 per group). (D) The AUC of CO_2 production in 12-h light and 12-h dark time after long-term HFD feeding ($n = 5$ or 6 per group; **, $P < 0.01$). (E) Heat generation profile of MMP14 Tg and WT mice in a 12-h light-dark cycle after long-term HFD feeding ($n = 5$ or 6 per group). (F) The AUC of heat generation in 12-h light and 12-h dark time after long-term HFD feeding ($n = 5$ or 6 per group; *, $P < 0.05$). (G) RER profile of MMP14 Tg and WT mice in a 12-h light-dark cycle after long-term HFD feeding ($n = 5$ or 6 per group). (H) The AUC (area under the curve) of RER in 12-h light and 12-h dark time after long-term HFD feeding ($n = 5$ or 6 per group, no difference between the groups). (I) Food intake of MMP14 Tg and WT mice in a 12-h light-dark cycle after long-term HFD feeding ($n = 5$ or 6 per group). (J) Activity profile of MMP14 Tg and WT mice in a 12-h light-dark cycle after long-term HFD feeding ($n = 5$ or 6 per group).

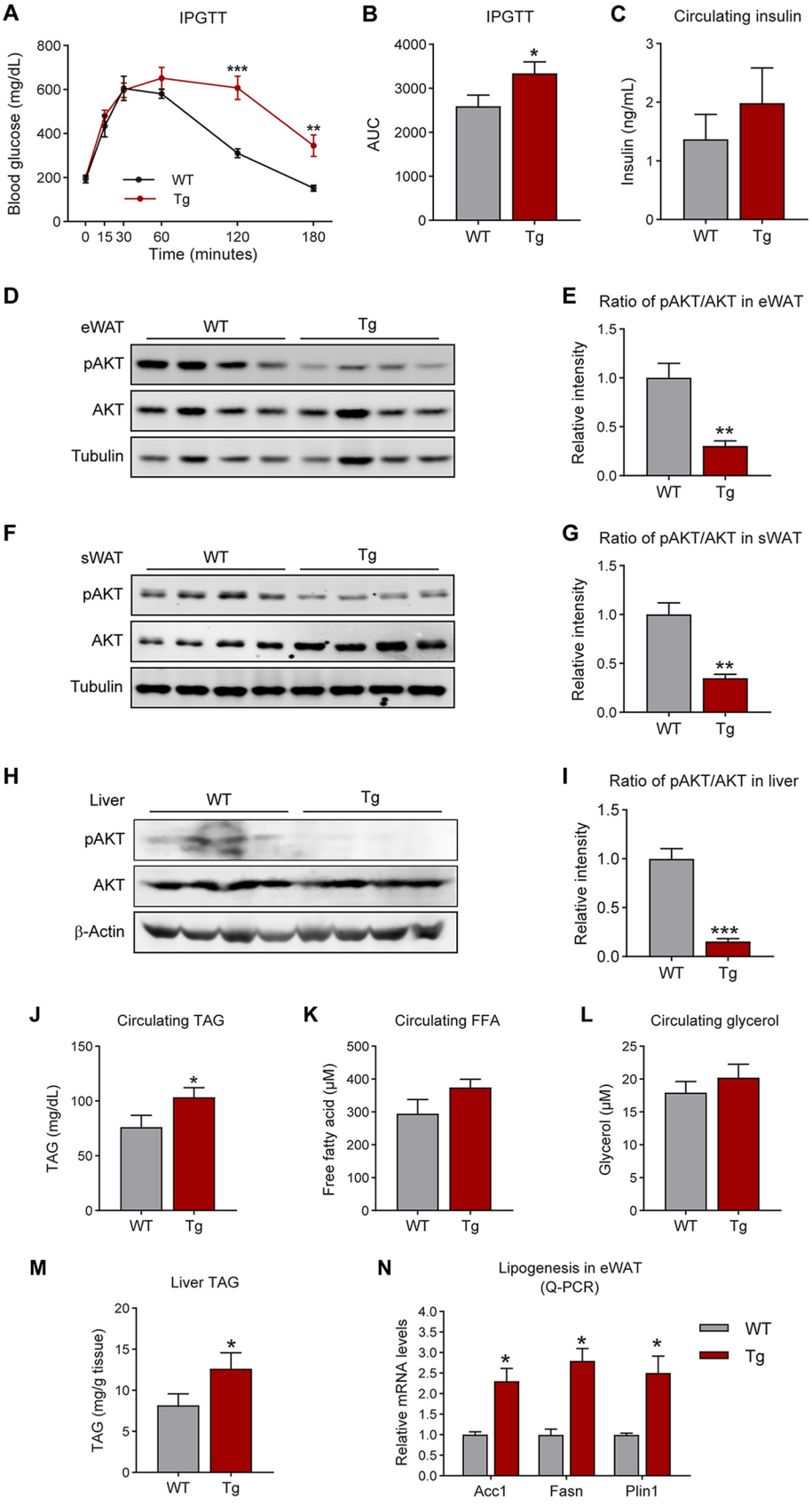

FIG 5 Overexpression of MMP14 in established obese adipose tissue leads to abnormal glucose and lipid metabolism in the transgenic mice. (A) IPGTT of MMP14 Tg and WT mice after a long-term HFD feeding

(Continued on next page)

macrophage accumulation around the adipocytes, are increased (Fig. 6T; quantification of the CLS numbers in Fig. 6U). In summary, overexpression of MMP14 in preexisting adipose tissue leads not only to fibrosis but also to local inflammation in the transgenic mice.

MMP14 digests COL6 to produce endotrophin, which triggers fibrosis and inflammation in obese adipose tissue. We next investigated the mechanisms governing MMP14 function on adipose tissue remodeling. Previously, we identified a small molecule called endotrophin which is derived from the carboxy terminus of COL6α3 (20). Endotrophin potently triggers local fibrosis and inflammation in obese adipose tissues (37). However, the responsible collagenase(s) remains unknown (37). Here, we propose that the deleterious effects of MMP14 are exerted via production of endotrophin. In support our hypothesis, we found that the parental COL6α3 chain is upregulated in MMP14-overexpressing adipose tissue (Fig. 6A and B). Furthermore, we identified the sequence Pro-Pro-Pro-Leu (PPPL) between the C4 and the C5 (endotrophin) domains at the carboxy terminus of COL6α3, matching the consensus cleavage site for MMP14 recognition (P-X-G/P-L) (Fig. 7A). To determine whether MMP14 directly digests COL6α3 at the indicated site, we generated a construct by fusing a prolactin signal sequence (plc) with the C4 and C5 domains of COL6α3 (Fig. 7B) and coexpressed Plc-C4-C5 with MMP14 in 293 cells. Western blotting revealed that upon cotransfection, endotrophin levels significantly increases in the medium, whereas the level of parental Plc-C4-C5 decreases (Fig. 7C). We then treated the cells with the MMP14 neutralizing antibody 3A2, and we found that endotrophin levels decrease upon the treatment of 3A2 at the dose of 1 μg/ml, while the level of parental Plc-C4-C5 increase (Fig. 7D). Importantly, we identified the endotrophin molecule in eWAT of the diet-induced obese mice by liquid chromatography-tandem mass spectrometry (LC-MS/MS) (Fig. 7E). Specifically, the MS data discovered three amino acid sequences with high fidelity. Combination of the three sequences reconstitutes most region of the endotrophin (Fig. 7E). Western blotting with anti endotrophin revealed that the endogenous endotrophin levels increase in the eWAT of the transgenic mice (Fig. 7F). Immunofluorescence staining (IF) further shows an enhanced endotrophin signal in the eWAT of the transgenic mice (Fig. 7G, left). Collectively, the results strongly suggest that MMP14 digests COL6α3 to produce endotrophin. Intriguingly, co-IF of anti endotrophin and anti-Mac2 (marker of macrophage) revealed not only more endotrophin and Mac2 signals but also significant colocalization of the signals in the eWAT (Fig. 7G), findings suggesting a positive correlation between endotrophin and macrophage accumulation.

Overexpression of MMP14 in early-stage obese adipose tissue brings about a metabolically healthy profile. Previously, we reported that adipose tissue-derived

FIG 5 Legend (Continued)
($n = 5$ per group, Student t test; **, $P < 0.01$; ***, $P < 0.001$). (B) AUC for the IPGTT performed in panel A ($n = 5$ per group, Student t test; *, $P < 0.05$). (C) Fasting circulating insulin levels in MMP14 Tg and WT mice after long-term HFD feeding ($n = 5$ per group, Student t test, no significant difference between the groups). (D) Western blotting of phospho-AKT (Ser473), total AKT, and tubulin in the eWAT of MMP14 Tg and WT mice after long-term HFD feeding ($n = 5$ per group, representative of three trials). (E) Quantification of the band density for the Western blotting in panel D indicating the ratio of phospho-AKT (Ser473) to total AKT ($n = 5$ per group, Student t test; **, $P < 0.01$). (F) Western blotting of phospho-AKT (Ser473), total AKT, and tubulin in the sWAT of MMP14 Tg and WT mice after long-term HFD feeding ($n = 5$ per group, representative of three trials). (G) Quantification of the band density of the Western blotting in panel F indicating the ratio of phospho-AKT (Ser473) to total AKT ($n = 5$ per group, Student t test; **, $P < 0.01$). (H) Western blotting of phospho-AKT (Ser473), total AKT, and β–Actin in the liver of MMP14 Tg and WT mice after long-term HFD feeding ($n = 5$ per group, representative of three trials). (I) Quantification of the band density of the Western blotting in panel H indicating the ratio of phospho-AKT (Ser473) to total AKT ($n = 5$ per group, Student t test; ***, $P < 0.001$). (J) Fasting circulating triacylglycerol (TAG) levels in MMP14 Tg and WT mice after long-term HFD feeding ($n = 5$ per group, Student t test; *, $P < 0.05$). (K) Fasting circulating free fatty acid (FFA) levels in MMP14 Tg and WT mice after a long-term HFD feeding ($n = 5$ per group, Student t test). (L) Fasting circulating glycerol levels in MMP14 Tg and WT mice after long-term HFD feeding ($n = 5$ per group, Student t test). (M) Triacylglycerol (TAG) levels in the liver of MMP14 Tg and WT mice after long-term HFD feeding ($n = 5$ per group, Student t test; *, $P < 0.05$). (N) Q-PCR analysis of lipogenesis-related genes, including *Accl*, *Fasn*, and *Plin1*, in the eWAT of MMP14 Tg and WT mice after long-term HFD feeding ($n = 5$ per group, Student t test; *, $P < 0.05$).

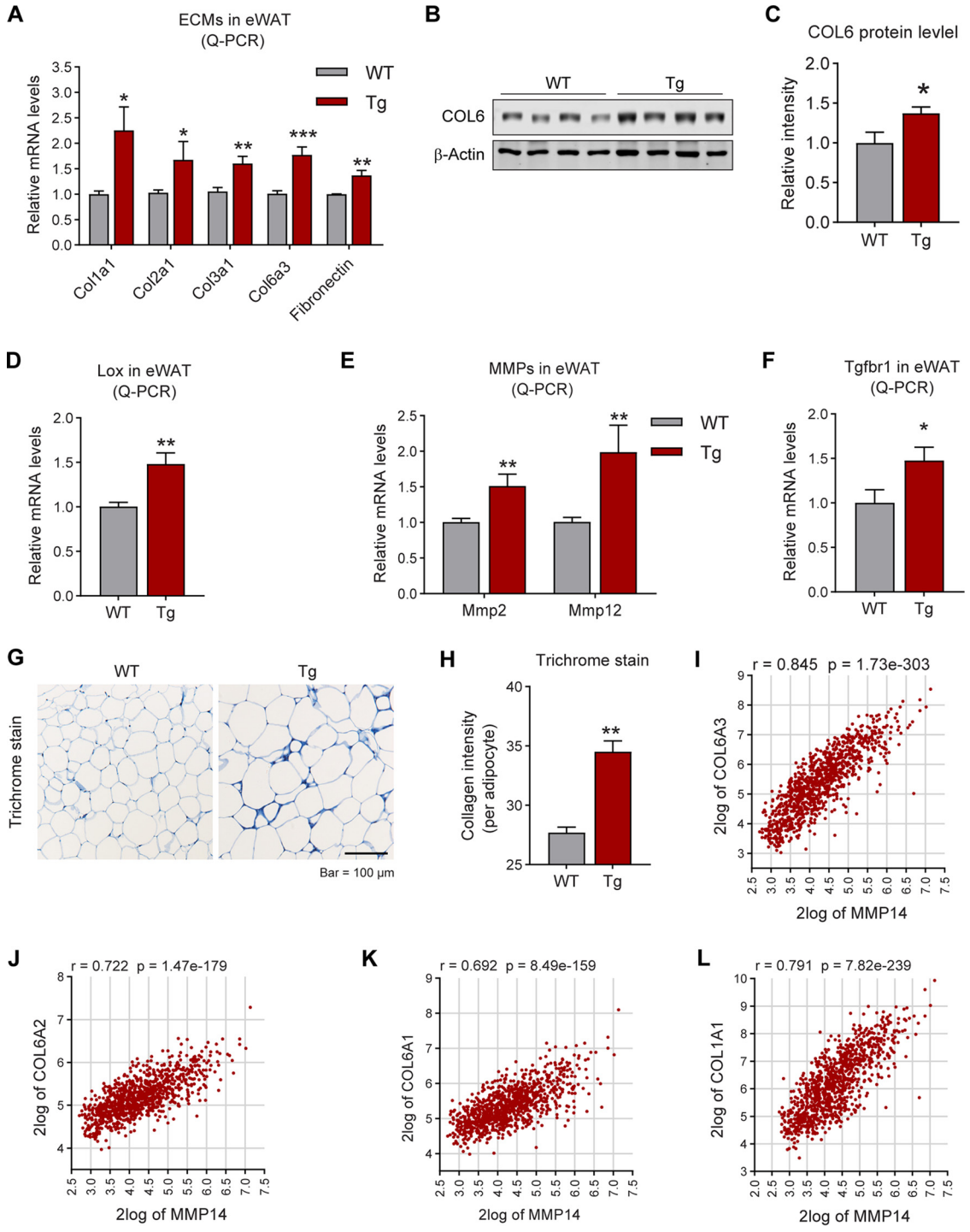

FIG 6 (Continued)

factors, such as VEGF-A, may have opposite effects at different stages during obesity (5). To determine whether MMP14 also displays such a dichotomous behavior, we took advantage of our inducible mouse model by inducing the overexpression of MMP14 at an early stage of obesity. Specifically, we treated transgenic mice and their littermate controls with a HFD combined with 200 mg/kg Dox for 8 weeks (Fig. 8A). In contrast to the results of the long-term HFD feeding, the MMP14 transgenic mice do not show differences in body weights, fat mass, and fat cell sizes (Fig. 8B to E). Unexpectedly, despite similar body weights between the groups, the transgenic mice exhibit en-

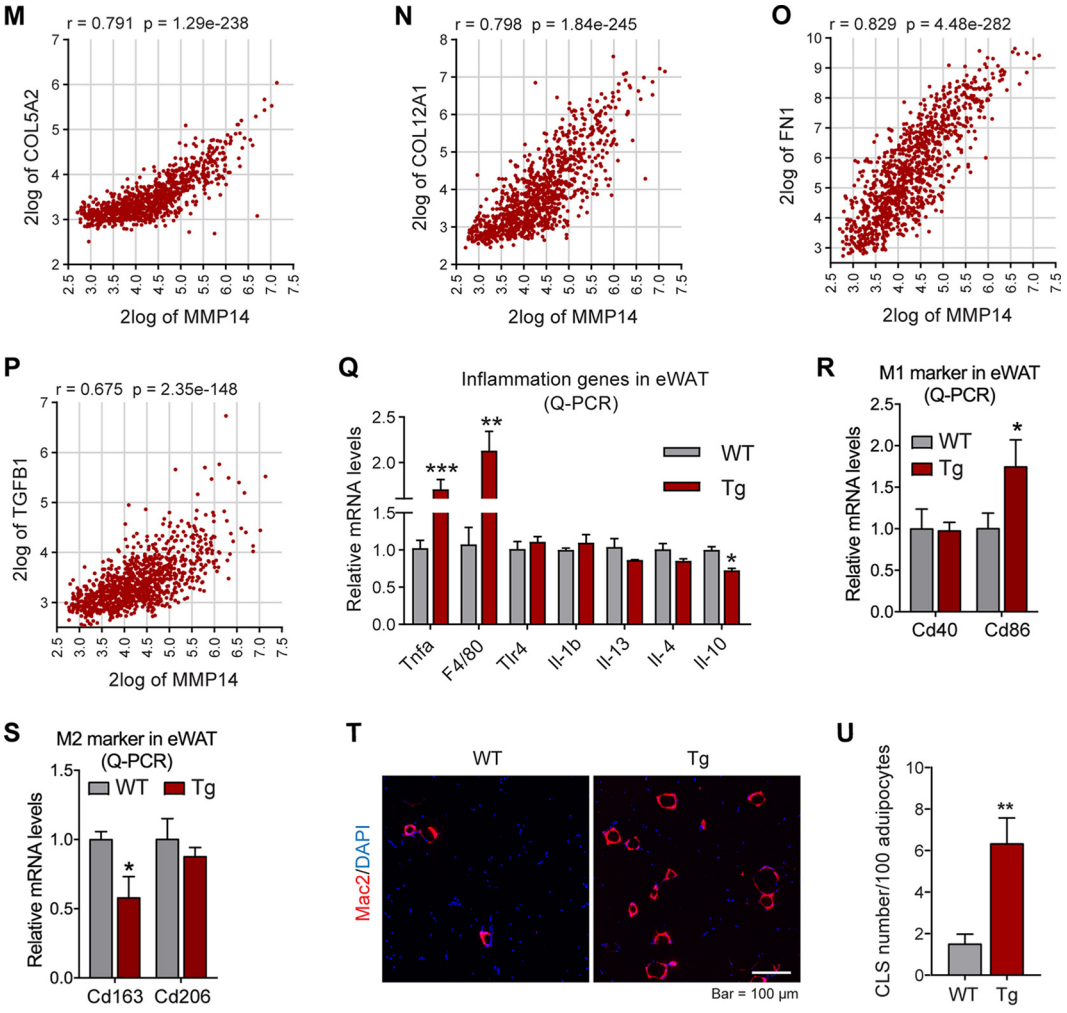

FIG 6 Overexpression of MMP14 in established obese adipose tissue stimulates local fibrosis and inflammation. (A) Q-PCR analysis of ECM-component genes, including *Col1a1*, *Col2a1*, *Col3a1*, *Col6a3*, and *Fibronectin*, in the eWAT of MMP14 Tg and WT mice after long-term HFD feeding ($n = 5$ per group, Student *t* test; *, $P < 0.05$; **, $P < 0.01$; ***, $P < 0.001$). (B) Western blotting of COL6 in the eWAT of MMP14 Tg and WT mice after long-term HFD feeding ($n = 5$ per group, representative of three trials). (C) Quantification of the band density of the Western blotting in panel B ($n = 5$ per group, Student *t* test; *, $P < 0.05$). (D) Q-PCR analysis of *Lox* (lysyl oxidase, a collagen linking enzyme) in the eWAT of MMP14 Tg and WT mice after long-term HFD feeding ($n = 5$ per group, Student *t* test; **, $P < 0.01$). (E) Q-PCR analysis of *Mmp2* and *Mmp12* in the eWAT of MMP14 Tg and WT mice after long-term HFD feeding ($n = 5$ per group, Student *t* test; **, $P < 0.01$). (F) Q-PCR analysis of *Tgfβr1* in the eWAT of MMP14 Tg and WT mice after long-term HFD feeding ($n = 5$ per group, Student *t* test; *, $P < 0.05$). (G) Trichrome staining of eWAT in the MMP14 Tg and WT mice after a long-term HFD feeding ($n = 5$ per group, representative of three trials). (H) Quantification of the density of dark blue in panel G ($n = 5$ per group, representative of three trials, Student *t* test; **, $P < 0.01$). (I to P) Correlation analysis between MMP14 and ECM genes, including COL6A3 (I), COL6A2 (J), COL6A1 (K), COL1A1 (L), COL5A2 (M), COL12A1 (N), FN1 (O), and TGFB1 (P), in the public breast tumor data set ($n = 1,110$) using genomics analysis and the visualization platform R2 (https://hgserver1.amc.nl/cgi-bin/r2/main.cgi). The correlation coefficient *r* value and the significance *P* value were autocalculated by the platform. (Q) Q-PCR analysis of proinflammatory and anti-inflammatory genes, including *Tnfα*, *F4/80*, *Tlr4*, *Il1β*, *Il13*, *Il4*, and *Il10*, in the eWAT of MMP14 Tg and WT mice after long-term HFD feeding ($n = 5$ per group, Student *t* test; *, $P < 0.05$; **, $P < 0.01$; ***, $P < 0.001$). (R) Q-PCR analysis of M1-phase macrophage markers, including *Cd40* and *Cd86*, in the eWAT of MMP14 Tg and WT mice after long-term HFD feeding ($n = 5$ per group, Student *t* test; *, $P < 0.05$). (S) Q-PCR analysis of M2-phase macrophage markers, including *Cd163* and *Cd206*, in the eWAT of MMP14 Tg and WT mice after long-term HFD feeding ($n = 5$ per group, Student *t* test; *, $P < 0.05$). (T) IF staining with anti-Mac2 antibody (marker of macrophage) in the eWAT of MMP14 Tg and WT mice after long-term HFD feeding. Nuclei were stained by DAPI (4′,6′-diamidino-2-phenylindole; $n = 5$ per group, representative of three trials). (U) Quantification of crown-like structures (CLS) formed by macrophage accumulation in panel T ($n = 5$ per group, Student *t* test; **, $P < 0.01$).

hanced glucose tolerance on IPGTT and enhanced insulin sensitivity during an insulin tolerance test (ITT) (Fig. 8F to I). The ITT results showing the percent basal glucose level also reveals a trend toward improved insulin sensitivity in transgenic mice (Fig. 8J and K). Furthermore, the levels of circulating triglycerides are decreased (Fig. 8L), indicating

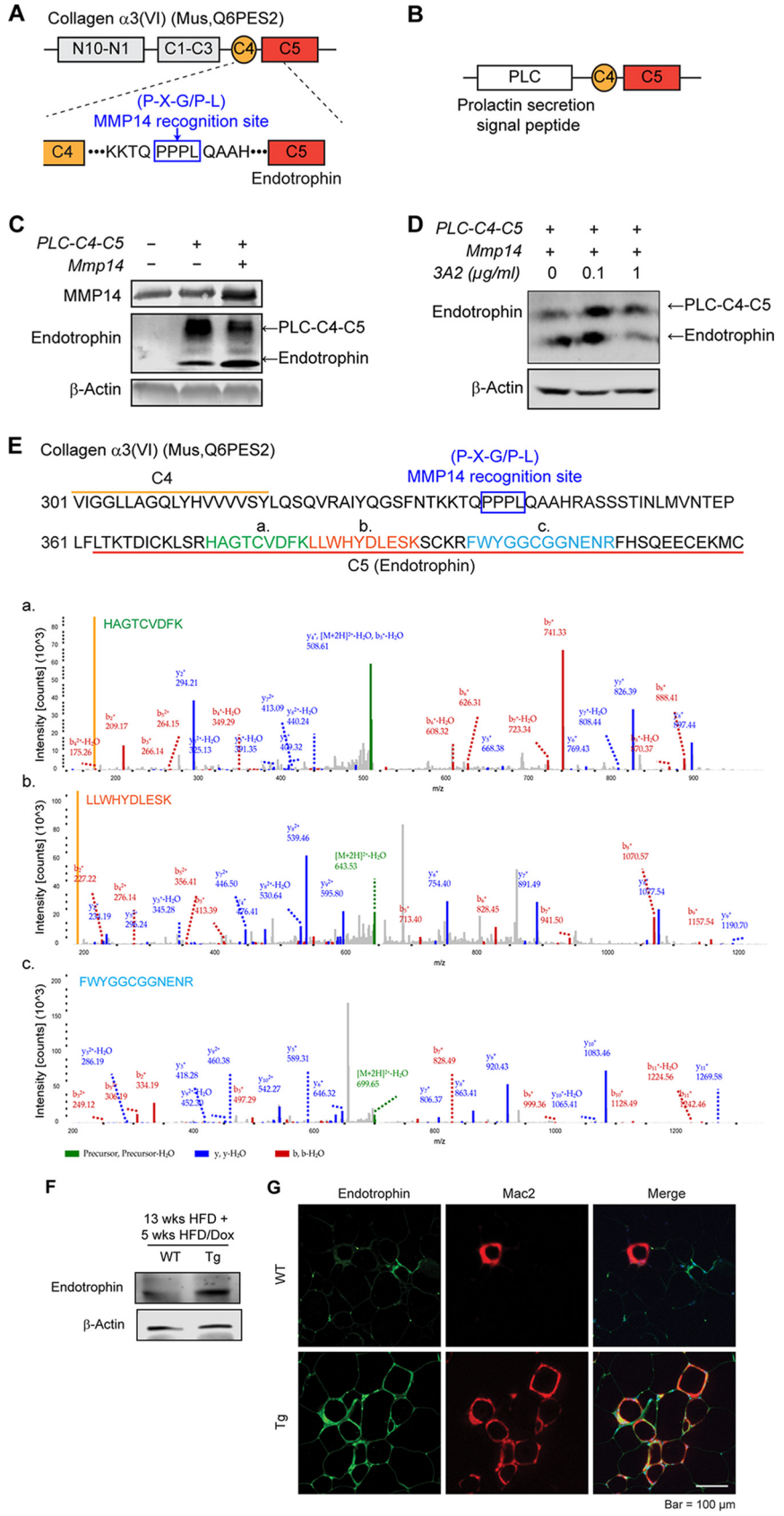

FIG 7 MMP14 digests COL6 to produce endotrophin, which triggers fibrosis and inflammation in obese adipose tissue. (A) Schematic diagram showing the protein domains of mouse COL6α3. The MMP14

(Continued on next page)

improved lipid metabolism in the transgenic mice. Q-PCR results show that fibrosis-related genes, such as *Tgfβ1*, *Col6α3*, and *Col1α1*, are downregulated in the eWAT of the transgenic mice (Fig. 8M). Western blotting further conformed the decreased protein level of COL6 (Fig. 8N; quantitative measurements in Fig. 8.O). Adiponectin gene expression is upregulated, while leptin gene expression does not significantly change (Fig. 8P). On the other hand, inflammation-related genes, such as *Il1β* and *F4/80*, are downregulated (Fig. 8Q). Interestingly, the M1-macrophage marker *Cd86* is downregulated (Fig. 8R), while the M2-macrophage markers, *Cd163* and *Cd206*, are upregulated (Fig. 8S), reflecting an anti-inflammatory microenvironment in the eWAT of the transgenic mice. Of note, Western blotting revealed that very low levels of endotrophin are detected in eWAT, and there is no difference between the transgenic mice and their littermate controls (Fig. 8T). In summary, overexpression of MMP14 in early-stage obese adipose tissue decreased the level of local fibrosis and inflammation. As the result, the mice exhibit improved glucose and lipid metabolism.

Based on these results, we proposed the following working model. During diet-induced obesity, local hypoxia induces HIF1α in adipose tissue. As a direct target of HIF1α, MMP14 is upregulated. At the early stage of obesity development, MMP14 digests collagens and prevents fibrosis, which promotes a healthy expansion of the adipose tissue. At the late stage of obesity, elevated levels of COL6 accumulate in adipose tissue. MMP14 digests the COL6α3 chain and produces endotrophin. The accumulation of endotrophin further shapes unhealthy microenvironment locally in the adipose tissue via triggering massive fibrosis and inflammation. The local pathological changes ultimately lead to systemic insulin resistance and other metabolic disorders (Fig. 8U).

DISCUSSION

Adipose tissue mass can expand rapidly during diet-induced obesity. Local hypoxia thus develops. HIF1α induced by hypoxia stimulates massive fibrosis locally in adipose tissue which may further leads to inflammation and systemic insulin resistance (1, 18). While it has been well accepted that fibrosis eventually leads to metabolic deficiencies, less attention has been given to understand the modifiers that regulate this pathological process in obese adipose tissue (47). Here, we reported that MMP14, the most enriched MMP in adipose tissue, plays a critical role in shaping unhealthy microenvironment in the preexisting obese fat pads. We discovered that MMP14 exerts its functions via digesting COL6α3, which is massively accumulated in the hypoxic adipose tissue, to produce endotrophin. Endotrophin, as a newly identified adipokine, functions as a costimulator, triggering fibrosis, macrophage accumulation, and inflammation, which eventually lead to systemic insulin resistance and other metabolic disorders (20, 37, 56). On the other hand, we reported here that MMP14 has the opposite function during early stage of obesity: it digests collagens to prevent overaccumulation of the ECM in fat pads, thereby facilitating a healthy expansion of fat pads. Of note, at this

FIG 7 Legend (Continued)
recognition site (P-X-G/P-L) between C4 and C5 domains is indicated within the blue box. (B) Schematic diagram showing the structure of pcDNA3.1-Plc-C4-C5 plasmid. The prolactin secretion signal peptide (Plc) was fused at the N terminus of the plasmid. (C) Western blotting of MMP14 and endotrophin in the 293T cells transfected with pcDNA3.1, Plc-C4-C5, or Plc-C4-C5, together with MMP14. β-Actin was used as loading control (representative of three experiments is shown). (D) Western blotting of endotrophin in 293T cells. The cells were cotransfected with Plc-C4-C5 and MMP14 and then treated with MMP14 monoclonal antibody 3A2 at the indicated doses. β-Actin was used as a loading control (representative of three trials). (E) Amino acid sequence of the C4-C5 terminal of COL6α3. Three peptides (indicated in green [a], orange [b], and blue [c]) which match parts of the sequence of C5 (endotrophin) were detected with high fidelity in the eWAT of HFD fed mice by mass spectrometry (LC-MS/MS). The MS spectra of three peptides were shown at the bottom. (F) Western blotting of endotrophin in the eWAT of MMP14 Tg and WT mice after long-term HFD feeding. The endotrophin was enriched from samples by immunoprecipitation with antiendotrophin antibody ($n = 5$ per group, representative of three trials). (G) Co-IF staining of endotrophin and Mac2 (marker of macrophage) in the eWAT of MMP14 Tg and WT mice after long-term HFD feeding. The right panel shows the colocalization of endotrophin and macrophages (indicated in yellow) ($n = 5$ per group, representative of three trials).

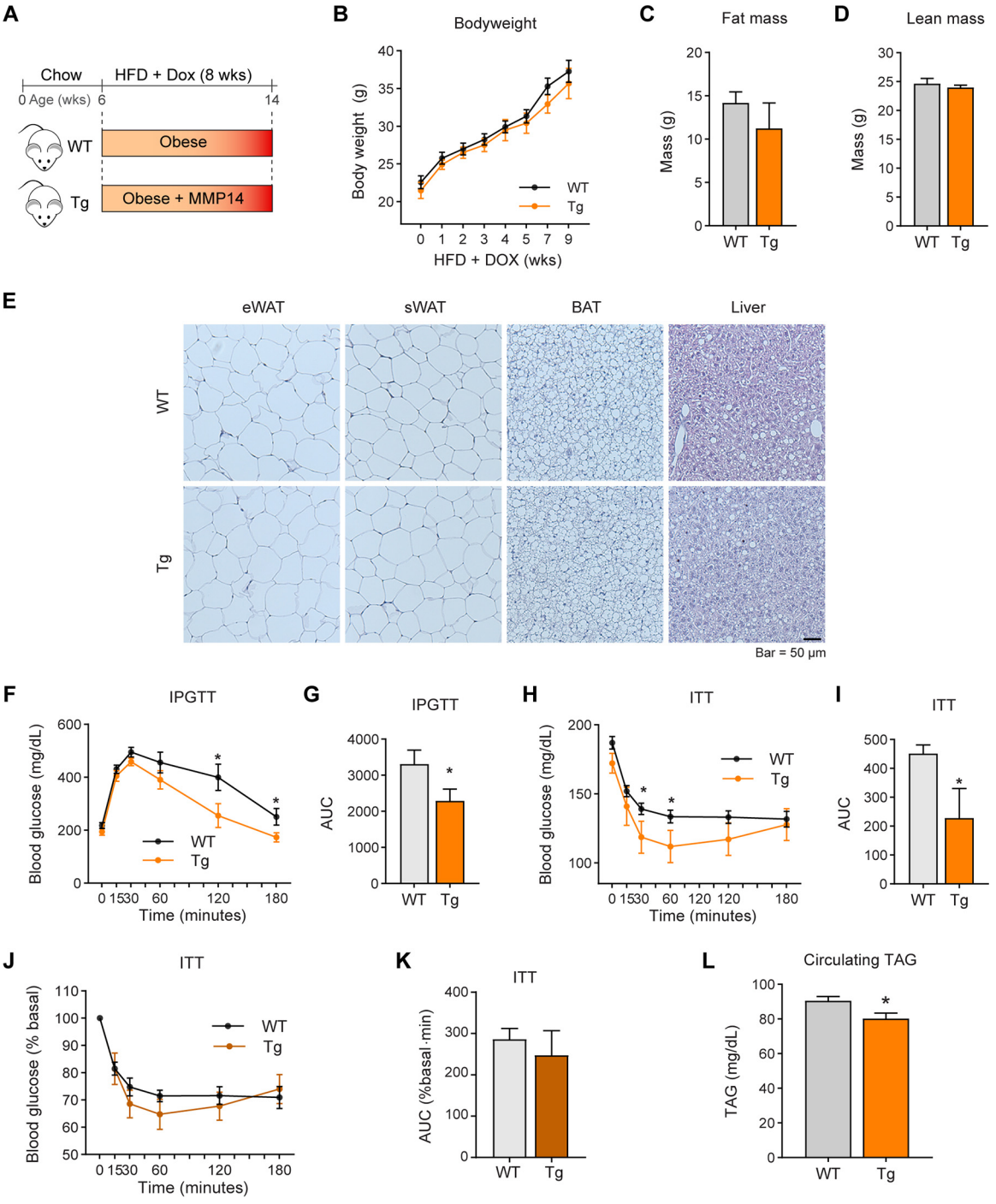

FIG 8 (Continued)

stage, COL6 and endotrophin have not accumulated to a significant degree to cause fibrosis and inflammation. Our study thus highlights the differential functions of MMP14 at different stages of obesity development and suggests that MMP14 inhibitors in the context of established obese adipose tissue might be an attractive therapeutic target to treat obesity-related metabolic diseases.

Previously we and others identified hypoxia as the initial step to trigger the sequential pathological changes in adipose tissue in response to diet-induced obesity (10–12, 14). We further found that HIF1α, induced by hypoxia, upregulates COL6, LOX, and IL-6 directly, which eventually lead to local fibrosis and inflammation (10, 14). In the

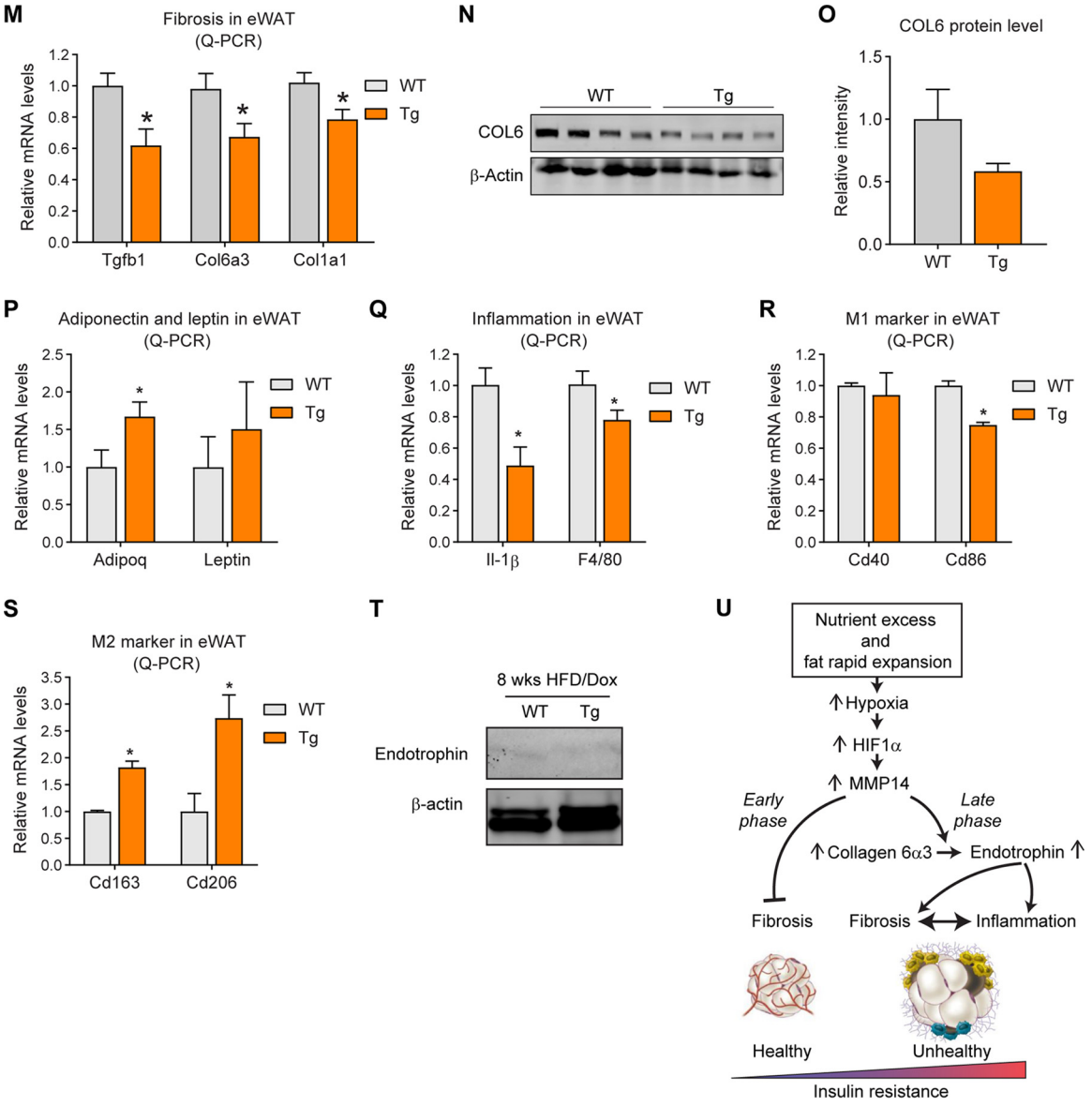

FIG 8 Overexpression of MMP14 in early-stage obese adipose tissue brings about metabolically healthy profile. (A) Schematic diagram showing the short-term HFD feeding program. The MMP14 Tg and WT mice were fed on HFD plus Dox (200 mg/kg diet) for 8 weeks. (B) Body weights of MMP14 Tg and WT mice during short-term HFD feeding ($n = 6$ per group, Student *t* test, no significant difference between the groups). (C) MRI analysis for fat mass of MMP14 Tg and WT mice after short-term HFD feeding ($n = 6$ per group, Student *t* test, no significant difference between the groups). (D) MRI analysis for lean masses of MMP14 Tg and WT mice after short-term HFD feeding ($n = 6$ per group, Student *t* test, no significant difference between the groups). (E) H&E staining of eWAT, sWAT, BAT, and liver in the MMP14 Tg and WT mice after short-term HFD feeding ($n = 6$ per group, representative of three trials). (F) IPGTT of MMP14 Tg and WT mice after short-term HFD feeding ($n = 6$ per group, Student *t* test; *, $P < 0.05$). (G) Area under the curve (AUC) for the IPGTT performed in panel F ($n = 6$ per group, Student *t* test; *, $P < 0.05$). (H) ITT of MMP14 Tg and WT mice after short-term HFD feeding ($n = 6$ per group, Student *t* test; *, $P < 0.05$). (I) AUC for the ITT performed in panel H ($n = 6$ per group, Student *t* test; *, $P < 0.05$). (J) The ITT result in panel H is shown as a percentage of the basal level ($n = 6$ per group, Student *t* test). (K) AUC for the graph presented in panel J ($n = 6$ per group, Student *t* test). (L) Fasting circulating triacylglycerol (TAG) levels in MMP14 Tg and WT mice after short-term HFD feeding ($n = 6$ per group, Student *t* test; *, $P < 0.05$). (M) Q-PCR analysis of ECM-component genes, including *Tgfβ1*, *Col6α3*, and *Col1α1*, in the eWAT of MMP14 Tg and WT mice after short-term HFD feeding ($n = 6$ per group, Student *t* test; *, $P < 0.05$). (N) Western blotting of COL6 in the eWAT of MMP14 Tg and WT mice after short-term HFD feeding ($n = 6$ per group, representative of three trials). (O) Quantification of the band density of the Western blotting in panel N ($n = 6$ per group, Student *t* test). (P) Q-PCR analysis of *Adiponectin* and *Leptin* in the eWAT of MMP14 Tg and WT mice after short-term HFD feeding ($n = 6$ per group, Student *t* test; *, $P < 0.05$). (Q) Q-PCR analysis of proinflammatory genes, including *Il1β* and *F4/80*, in the eWAT of MMP14 Tg and WT mice after short-term HFD feeding ($n = 6$ per group, Student *t* test; *, $P < 0.05$). (R) Q-PCR analysis of M1-phase macrophage markers, including *Cd40* and *Cd86*, in the eWAT of MMP14 Tg and WT mice after short-term HFD feeding ($n = 6$ per group, Student *t* test; *, $P < 0.05$). (S) Q-PCR analysis of M2-phase macrophage markers, including *Cd163* and *Cd206*, in the eWAT of MMP14 Tg and WT mice after short-term HFD feeding ($n = 6$ per group, Student *t* test; *, $P < 0.05$). (T) Western blotting of endotrophin in the eWAT of MMP14 Tg and WT mice after short-term HFD feeding. The endotrophin molecules were enriched from samples by immunoprecipitation with antiendotrophin antibody ($n = 6$ per group, representative of three trials). (U) Proposed working model of the study. During diet-induced obesity, local hypoxia induces HIF1α in adipose tissue. As a direct target of HIF1α,

(Continued on next page)

present study, we discovered for the first time that another important fibrotic factor, MMP14, is a novel HIF1 target. MMP14 has been reported to be the major MMP in adipose tissue (49, 50). Many other MMPs, such as MMP2, MMP12, and MMP19, all of which play important roles in ECM remodeling in adipose tissue, are the downstream substrates for MMP14 (48). Previous studies revealed that MMP14 stimulates adipocyte differentiation in the neonate and hence promotes adipose tissue expansion (48). However, little is known about its exact role in the ECM remodeling during obesity. In that sense, our study is timely and novel. Particularly, we reported that MMP14 increases in response to obesity development. We took advantage of the public genomic information and found that the increased levels of MMP14 show a tight correlation with multiple fibrotic proteins, especially COL6. Furthermore, mechanistically, we unraveled that in the established obese adipose tissue, MMP14 digests COL6α3 chain to produce endotrophin, which leads to a very unhealthy environment by triggering fibrosis and inflammation.

Endotrophin is produced during obesity development (37). It has been reported not only to have deleterious effects on adipose tissue remodeling but also to promote tumor growth and other pathological changes in the heart and kidney (20, 37–40). Here, we identified MMP14 as the key collagenase to produce endotrophin. Furthermore, we identified the cleavage site in COL6α3 for MMP14, and we verified this site in cells. More importantly, we confirmed the production of endotrophin in obese adipose tissue by MS. Of note, even though MMP14 is the major collagenase in adipose tissue, we cannot rule out the potential involvement of other proteolytic enzymes to produce endotrophin. For example, another group recently used isotopic MS-based analysis and found that the extracellular metalloproteinase named bone morphogenetic protein 1 (BMP-1) is also involved in endotrophin release (57). Moreover, the cleavage site of human endotrophin has also been reported recently (39).

Adipose tissue remodeling is a dynamic process orchestrated by multiple pathological changes. Many molecules play critical roles in the expansion (1). These molecules may exert opposite functions during different stages of obesity development. Previously, we reported that VEGF-A, the only bona fide angiogenetic factor in adipose tissue, plays dichotomous roles in adipose tissue physiology/pathology during obesity. At an early stage of adipose tissue expansion, VEGF-A exerts beneficial effects by stimulating angiogenesis to provide oxygen, nutrition, stem cells, and other important factors, thereby preventing hypoxia and facilitating "healthy" expansion (5, 58, 59). At the late stage, VEGF-A overexpression leads to an inflammatory microenvironment, which triggers systemic insulin resistance (5). In the present study, we identified MMP14 as another factor that displays such a dichotomous function. At early stage of obesity, MMP14 is upregulated by HIF1α. It exerts an antifibrotic function by digesting fibrotic molecules, particularly collagen proteins. Since collagen do not reach very high levels at this stage, endotrophin is almost undetectable; at the late stage of obesity, MMP14 expression is maintained at a relatively high level or even increased more. Meanwhile, COL6, along with other fibrotic components, accumulate to a much higher level as part of the ECM expansion. Digestion of COL6 by MMP14 generates endotrophin, which triggers massive fibrosis and inflammation to shape an unhealthy microenvironment. Our studies demonstrate that adipose tissue remodeling is a process with multiple molecules exerting divergent effects during different stages of tissue expansion.

In conclusion, findings from our study enhance the general understanding of the complexity of adipose tissue physiology and highlight the critical role of MMP14 in adipose tissue remodeling. The findings demonstrate that MMP14 and the resulting

FIG 8 Legend (Continued)
MMP14 is upregulated. At the early stage of obesity development, MMP14 digests collagens and prevents fibrosis, which then promotes healthy expansion of the tissue. At the late stage of obesity, tremendous amounts of COL6 accumulate in adipose tissue. MMP14 digests COL6α3 chain and produces endotrophin. Accumulation of endotrophin further shapes unhealthy microenvironment locally in the adipose tissue by triggering massive fibrosis and inflammation. The local pathological changes ultimately lead to systemic insulin resistance and other metabolic disorders.

enhanced levels of endotrophin bear great promise from a therapeutic perspective for obesity and obesity-related metabolic diseases.

MATERIALS AND METHODS

Chemicals and reagents. Chemicals and reagents were purchased from following sources. Anti-MMP14 (ab51074) and antitubulin (catalog no. ab210797) antibodies were from Abcam. Anti-pAKT (catalog no. 9271) and anti-AKT (catalog no. 272) antibodies were from Cell Signaling Technology. Anti-HIF1α (AF1935), anti-β-actin (MAB8929) antibodies, and goat IgG (AB-108-C) were from R&D Systems. Anti-MAC2 antibody (eBioM3/38) and the agarose ChIP kit (catalog no. 26156) were from Thermo Fisher Scientific. Doxycycline (D9891), $CoCl_2$ (catalog no. 60818), the Masson's trichrome staining kit (HT15-1KT), and the glucose oxidase/peroxidase kit (GAGO-20) were from Sigma-Aldrich. PX-478 (catalog no. 10005189) and the triglyceride colorimetric assay kit (catalog no. 10010303) were from Cayman Chemical. The free fatty acid assay kit (EFFA-100) and the glycerol assay kit (EGLY-200) were from Bioassay Systems. Anti-MMP14 monoclonal antibody (3A2) was the gift from X. Ge's group at the University of California, Riverside (60). Antiendotrophin antibody has been described previously (37).

Animals. All the animal experiments were reviewed and approved by the Animal Welfare Committee of University of Texas Health Science Center at Houston (animal protocol AWC-18-0057). Mice were housed in animal facility under 12-h light-dark cycle at 22 $\pm$ 1°C. The mice had *ad libitum* access to water and regular chow diet, unless indicated otherwise. C57BL/6J (stock 000664) was purchased from The Jackson Laboratory. The TRE-Mmp14-tTS transgenic line was generated on a pure C57BL/6J background by the Transgenic and Stem Cells Service Center at University of Texas Health Science Center at Houston. Plasmids pUHG10.3-TetO-Mmp14-flag and pTet-tTS were comicroinjected into the fertilized single-cell mouse embryos. After injection, the eggs were surgically transferred to pseudopregnant foster mothers. Seven founder mice carrying two transgenes (TRE-Mmp14-Flag; tTS strain) were identified from the offspring. Apn-rtTA; TRE-Mmp14-Flag; tTS transgenic (Tg) mice (MMP14 Tg) were obtained by crossing TRE-Mmp14; tTS strain with the Apn-rtTA transgenic strain. The mice carrying only the Apn-rtTA transgene were used as controls (WT). For characterization, the MMP14 Tg and WT mice were fed on regular chow diet with doxycycline (Dox; 200 mg/kg diet) for 1 week. Among the seven strains, the line with highest MMP14 overexpression level in adipose tissue was selected and used in the study. For the long-term high-fat-diet (HFD) feeding, the MMP14 Tg and their littermate control mice were fed on HFD (60 kcal% fat, research diet, catalog no. D12492) for 13 weeks, followed by continuously feeding on HFD plus Dox (200 mg/kg diet) for 5 more weeks. For the short-term HFD feeding, the MMP14 Tg and their littermate control mice were fed on HFD plus Dox (200 mg/kg diet) for 8 weeks. For HIF1α inhibitor treatment, WT C57BL/6J mice were fed on regular chow diet or HFD together with or without PX-478 (specific HIF1α inhibitor; 5 mg/kg [body weight]) treatment every other day for 5 weeks.

Indirect calorimetric measurements. Indirect calorimetry analysis was performed in TSE metabolic chambers (TSE Systems, Chesterfield, MO). The MMP14 Tg mice and their littermate controls were individually housed in the metabolic chambers and maintained under a 12-h light/dark cycle with light on from 7:00 a.m. to 7:00 p.m. All of the mice had *ad libitum* access to water and HFD plus Dox during the measurements. The metabolic profiles, including O_2 consumption (milliliters per kilogram per hour), CO_2 generation (milliliters per kilogram per hour), heat generation (kilocalories per kilogram per hour), respiratory exchange rate (RER; VCO_2/VO_2), food intake (grams), and movements (counts), were continuously recorded. The data of O_2 consumption, CO_2 generation, and heat generation were normalized to subject body weight. The data for day 2 to day 4 were recorded and analyzed.

Body composition. The total body mass as well as fat mass and lean mass of mice were measured by an Echo 3-in-1 nuclear magnetic resonance Minispec magnetic resonance imaging (MRI) instrument (EchoMRI, Houston, TX).

IPGTTs and ITTs. An intraperitoneal (i.p.) glucose tolerance test (IPGTT) and an insulin tolerance test (ITT) were performed as previously described (37). For the IPGTT, the mice were fasted for 4 h before i.p. injection of glucose (2.5 g/kg [body weight]). At the indicated time points, tail blood samples were collected with heparin-coated capillary tubes and centrifuged at 6,000 rpm for 6 min. The glucose levels in plasma were measured by the glucose oxidase/peroxidase method. For the ITT, the mice were fasted for 4 h before i.p. injection of insulin (0.75 U/kg [body weight]). At the indicated time points, tail blood samples were collected with heparin-coated capillary tubes and centrifuged at 6,000 rpm for 6 min, followed by glucose measurement.

Measurements of insulin, TAG, FFA, and glycerol. After the mice were fasted for 4 h, tail blood samples were collected with heparin-coated capillary tubes and centrifuged at 6,000 rpm for 6 min to obtain plasma. The levels of insulin, triglyceride (TAG), free fatty acid (FFA), and glycerol in plasma were measured by kits according to the manufacturer's instructions.

DNA construction. The construction of pcDNA3.1-Mmp14 was generated by cloning the full length of cDNA of mouse *Mmp14* into vector of pcDNA3.1. The construction of pcDNA3.1-Plc-C4-C5 was generated by cloning the cDNA of prolactin signal sequence and C4-C5 terminal of *Col6a3* (beginning in the middle of C4 domain) into vector of pcDNA3.1.

3A2 IgG production. A 3A2 heavy-chain (HC) expression cassette including a chimeric intron, secrete signal, HC gene, and WPRE (woodchuck hepatitis virus posttranscriptional regulatory element) was cloned into pcDNA carrying a zeocin marker between the cytomegalovirus enhancer/promoter and bGH poly(A). Similarly, a 3A2 light-chain (LC) expression vector with hygromycin resistance was constructed. Human HEK293F cells were maintained in Gibco Expi293 expression medium (Life Technology) at 37°C and 8% CO_2 in a humidified atmosphere with orbital shaking at 135 rpm. For transfection, 2×10^6 293F cells were incubated with 1 μg of HC and 1 μg of LC expression vectors and 6 μg of PEI MAX 40K

(Polysciences) for 24 h. Stable cell lines were selected in fresh medium supplemented with 500 μg/ml zeocin and 350 μg/ml hygromycin for 8 days and then with 100 μg/ml zeocin and 50 μg/ml hygromycin for 15 days. For 3A2 IgG expression, 1×10^6/ml cells were cultured in Expi293 medium with 100 μg/ml zeocin and 50 μg/ml hygromycin for 7 days. 3A2 IgG was purified from collected culture medium by protein A affinity chromatography. Produced 3A2 IgG was characterized by SDS-PAGE and MMP-14 inhibition assay.

Cell culture and drug treatments. 293T cells (CRL-3216) and PC3 cells (CRL-1435) were purchased from the American Type Culture Collection and maintained in Dulbecco modified Eagle medium supplemented with 10% fetal bovine serum in a humidified atmosphere of 5% CO_2 at 37°C. For cotransfection, when grown to 80% confluence, 293T cells were transfected with pcDNA3.1-Mmp14 along with or without pcDNA3.1-Plc-C4-C5. At 48 h after transfection, the cells were harvested to analyze the endotrophin levels. For MMP14 monoclonal antibody treatment, different doses of 3A2 (0, 0.1, and 1 μg/ml) were added to cell culture media 6 h after transfection until collection for analysis. For hypoxia assay, 100% confluent PC3 cells were pretreated with 100 μM $CoCl_2$ for 2 h, followed by cotreatment of 100 μM $CoCl_2$ and 30 μM PX-478 for 4 h. The cells were then harvested for analysis of MMP14 levels.

Gene correlation analyses of public human genome database. Gene correlation analyses were performed in public genomics analysis and visualization platform R2 (https://hgserver1.amc.nl/cgi-bin/r2/main.cgi), and the data were prepared using GraphPad Prism 8. The correlation analyses were based on the public database Tumor Breast (Nurses Health Study I and II, set a)-Heng-1110-rma-hta2t ($n = 1{,}110$). The Pearson correlation coefficient (r value) and statistical significance (P value) were calculated within the platform.

ChIP assay. The ChIP assay was performed following the instruction of Pierce Agarose ChIP kit (Thermo Fisher Scientific, catalog no. 26516). Briefly, after 95% confluence, PC3 cells were incubated in a hypoxia chamber for 8 h. The cells were then cross-linked using 1% formaldehyde at room temperature for 10 min, followed by quenching with glycine (final concentration, 0.125 M) for 10 min. For adipose tissues, 100 mg of frozen eWAT was cut into slices thinner than 1 mm and fixed in 1% formaldehyde in phosphate-buffered saline (PBS) for 10 min at room temperature. The tissue was then quenched with glycine (final concentration, 0.125 M) for 10 min and washed twice with chilly PBS containing EDTA-free proteinase inhibitor. Afterward, the samples were collected and homogenized in cell lysis buffer I with a Dounce homogenizer on ice to generate a homogenous cell slurry. The cell slurry was centrifuged at 9,000 $\times$ g for 10 min at 4°C to precipitate the cell nuclei. The supernatant was then removed, and cell nuclei were resuspended in 100 μl of MNase digestion buffer working solution. To shear the DNA, the nuclear suspension was added with 0.25 μl of micrococcal nuclease and incubated at 37°C for 15 min followed by adding 10 μl stopping solution. To recover the nuclei, the sample was centrifuged at 9,000 $\times$ g, and the nuclear pellet was responded in 100 μl of lysis buffer 2. After incubation 15 min on ice, the sample was centrifuged at 9,000 $\times$ g for 5 min, and the supernatant containing digested chromatin was collected. For each immunoprecipitation, 50 μl of the digested chromatin, together with 10 μg of anti-HIF1α antibody or IgG and A/G plus agarose, was added to the immunoprecipitation dilution buffer, followed by incubation at 4°C overnight. After the agarose resin was washed with wash buffer three times, the DNAs were eluted from the agarose beads, and then 20 ng of DNAs was used as the template for the PCR or quantitative PCR (Q-PCR) reaction. The primers used for ChIP-PCR were as follows: P1-F, 3′-CTGGTTCCATTCCAGTTCAGC-5′; P1-R, 3′-ATAGTTGGGCTAGTCCTATGGC-5′; P2-F, 3′-CCTTCACGTTCCCCATCTGT-5′, P2-R, 3′-GCTAGTCCTATGGCCTGCAA-5′; P3-F, 3′-ACCTCCTTTGCAGGCCATA-5′; P3-R, 3′-CTTCCCAGTGGGGGTAACCT-5′; P4-F, 3′-AGGACTAGCCCAACTATGAGAA-5′; P4-R, 3′-GACACCAGATGCTTGCCAAAA-5′; P5-F, 3′-GGCAAGCATCTGGTGTCAGT-5′; P5-R, 3′-TTTTCAGGTCCTGTGGAGCC-5′; P6-F, 3′-GAGGTTACCCCCACTGGGAA-5′; and P6-R, 3′-AGCTACCTACCCCACAGTGA-5′. The negative-control primer for ChIP was used as previously described (61).

Quantitative PCR analysis. Q-PCR analysis was performed as described previously (62). Briefly, total RNAs were extracted using TRIzol reagent (Thermo Fisher Scientific) and an Illustra RNAspin minikit (GE Healthcare Life Sciences). Next, 1 μg of RNA was used to reverse-transcribe into cDNAs with RevertAid reverse transcription kit (Thermo Fisher Scientific). Q-PCR was carried out on Bio-Rad CFX96 system (Bio-Rad Laboratories). The results were calculated using the $2^{-\Delta\Delta CT}$ method and normalized using 18S RNAs. The primer sequences were described previously (37).

Western blotting. Protein samples were prepared from adipose tissues as described previously (62). Proteins were separated by SDS-PAGE and then transferred to a polyvinylidene difluoride membrane. The membranes were blocked with 5% fat-free milk and incubated with primary antibodies at 4°C overnight. After three washes with 0.5% Tween 20 in Tris-buffered saline, the blots were probed with fluorescent-dye-conjugated secondary antibodies at room temperature for 1 h protected from light. After three more washes, the blots were visualized by using Odyssey imaging system (LI-COR). Equal loading was ensured by using anti-β-tubulin or anti-α-actin antibodies.

To analyze the endotrophin level in the adipose tissues of WT and Tg mice, clear supernatants of adipose tissue were incubated with antiendotrophin antibody and A/G agarose at 4°C overnight. After the agarose resin was washed three times, the enriched endotrophin was eluted off from the agarose beads and analyzed by Western blotting.

Mass spectrometry. Endotrophin was enriched from obese adipose tissues by immunoprecipitation with antiendotrophin antibody as described above. The samples were separated by SDS-PAGE and analyzed by LC-MS/MS at the Clinical and Translational Proteomics Service Center at UTHealth, as described previously (63). Briefly, after in-gel digestion, the samples were extracted and analyzed on an Orbitrap Fusion Tribrid mass spectrometer (Thermo Scientific). The sequences of the peptides were

analyzed by using a data-dependent acquisition method (63). The peptides with an ion score of >20 were considered to be high fidelity.

Histology. The adipose tissues and liver were collected and fixed in PBS-buffered 10% formalin for 48 h at room temperature. After paraffin embedding, the tissues were divided into 5-μm sections and deparaffinized for use. For hematoxylin and eosin (H&E) staining, the deparaffinized tissue sections were stained according to standard protocols and imaged under a light microscope. The numbers and sizes for adipocytes were quantified basing on the H&E staining images using ImageJ software. For Masson's trichrome staining, the deparaffinized adipose tissue sections were stained according to the manufacturer's instructions (Sigma, HT15-1KT). The quantification of the dark blue density was performed using ImageJ software. For immunofluorescent staining, the tissue sections were further processed with permeabilization and antigen retrieval after deparaffinization. The samples were then blocked with 1% bovine serum albumin at room temperature for 1 h, followed by incubation with primary antibodies at 4°C overnight (ca. 1:100 to 1:200 diluted in blocking buffer). After three washes, the sections were incubated with fluorescence-conjugated secondary antibodies (1:100 diluted in blocking buffer) at room temperature for 1 h protected from the light. After another three washes, the sections were mounted with antifade media and visualized under a fluorescence microscope.

Statistical analysis. All data are presented as means ± the standard errors of the mean (SEM). Statistical analyses were performed by using GraphPad Prism 8 software. An unpaired Student *t* test was used for statistical significance analysis when two groups were compared. One- or two-way analysis of variance (ANOVA) was use for the comparisons among multiple groups. A P value of <0.05 was considered to be statistically significant. For Pearson correlation analysis of the data set from the patients, the Pearson correlation coefficient (r value) and statistical significance (P value) were calculated using the tools provided within the platform (https://hgserver1.amc.nl/cgi-bin/r2/main.cgi).

ACKNOWLEDGMENTS

We thank Yuanzhong Xu and Qingchun Tong in the Center for technical support. We also thank Zhengmei Mao in the microscopy core of the Institute of Molecular Medicine for assistance in imaging and tissue processing, as well as Li Li at the Clinical and Translational Proteomics Service Center at the University of Texas Health Science Center for the LC-MS/MS analysis.

This study was supported by National Institutes of Health grant R01DK109001 (to K.S.). This study was also supported in part by Cancer Prevention and Research Institute of Texas (PR150551 to Z.A.) and the Welch Foundation (AU-0042-20030616 to Z.A.). This study was also supported in part by the Clinical and Translational Proteomics Service Center at the University of Texas Health Science Center.

Author contributions: conceptualization, K.S.; methodology, K.S., P.E.S., X.L., Y.Z., C.C., and X.G.; investigation, X.L., Y.Z., C.C., L.Y., H.-H.L., N.Z., M.G.K., Z.A., P.E.S., and K.S.; writing—original draft, K.S.; writing—review and editing, P.E.S., X.L., Z.A.; and resources, K.S., P.E.S., C.C., and Z.W.

We declare that we have no competing financial interests.

REFERENCES

1. Sun K, Kusminski CM, Scherer PE. 2011. Adipose tissue remodeling and obesity. J Clin Invest 121:2094–2101. https://doi.org/10.1172/JCI45887.
2. Halberg N, Wernstedt-Asterholm I, Scherer PE. 2008. The adipocyte as an endocrine cell. Endocrinol Metab Clin North Am 37:753–768. https://doi.org/10.1016/j.ecl.2008.07.002.
3. Ye J, Gao Z, Yin J, He Q. 2007. Hypoxia is a potential risk factor for chronic inflammation and adiponectin reduction in adipose tissue of *ob/ob* and dietary obese mice. Am J Physiol Endocrinol Metab 293:E1118–E1128. https://doi.org/10.1152/ajpendo.00435.2007.
4. Unger RH, Scherer PE, Holland WL. 2013. Dichotomous roles of leptin and adiponectin as enforcers against lipotoxicity during feast and famine. Mol Biol Cell 24:3011–3015. https://doi.org/10.1091/mbc.E12-10-0774.
5. Sun K, Wernstedt Asterholm I, Kusminski CM, Bueno AC, Wang ZV, Pollard JW, Brekken RA, Scherer PE. 2012. Dichotomous effects of VEGF-A on adipose tissue dysfunction. Proc Natl Acad Sci U S A 109:5874–5879. https://doi.org/10.1073/pnas.1200447109.
6. Cao Y. 2007. Angiogenesis modulates adipogenesis and obesity. J Clin Invest 117:2362–2368. https://doi.org/10.1172/JCI32239.
7. Elias I, Franckhauser S, Ferre T, Vila L, Tafuro S, Munoz S, Roca C, Ramos D, Pujol A, Riu E, Ruberte J, Bosch F. 2012. Adipose tissue overexpression of vascular endothelial growth factor protects against diet-induced obesity and insulin resistance. Diabetes 61:1801–1813. https://doi.org/10.2337/db11-0832.
8. Cao R, Brakenhielm E, Wahlestedt C, Thyberg J, Cao Y. 2001. Leptin induces vascular permeability and synergistically stimulates angiogenesis with FGF-2 and VEGF. Proc Natl Acad Sci U S A 98:6390–6395. https://doi.org/10.1073/pnas.101564798.
9. Cao Y. 2013. Angiogenesis and vascular functions in modulation of obesity, adipose metabolism, and insulin sensitivity. Cell Metab 18:478–489. https://doi.org/10.1016/j.cmet.2013.08.008.
10. Halberg N, Khan T, Trujillo ME, Wernstedt-Asterholm I, Attie AD, Sherwani S, Wang ZV, Landskroner-Eiger S, Dineen S, Magalang UJ, Brekken RA, Scherer PE. 2009. Hypoxia-inducible factor 1alpha induces fibrosis and insulin resistance in white adipose tissue. Mol Cell Biol 29:4467–4483. https://doi.org/10.1128/MCB.00192-09.
11. Yin J, Gao Z, He Q, Zhou D, Guo Z, Ye J. 2009. Role of hypoxia in obesity-induced disorders of glucose and lipid metabolism in adipose tissue. Am J Physiol Endocrinol Metab 296:E333–E342. https://doi.org/10.1152/ajpendo.90760.2008.
12. He Q, Gao Z, Yin J, Zhang J, Yun Z, Ye J. 2011. Regulation of HIF-1α activity in adipose tissue by obesity-associated factors: adipogenesis, insulin, and hypoxia. Am J Physiol Endocrinol Metab 300:E877–E885. https://doi.org/10.1152/ajpendo.00626.2010.
13. Krishnan J, Danzer C, Simka T, Ukropec J, Walter KM, Kumpf S, Mirtschink P, Ukropcova B, Gasperikova D, Pedrazzini T, Krek W. 2012. Dietary obesity-associated Hif1α activation in adipocytes restricts fatty acid

oxidation and energy expenditure via suppression of the Sirt2-NAD$^+$ system. Genes Dev 26:259–270. https://doi.org/10.1101/gad.180406.111.
14. Sun K, Halberg N, Khan M, Magalang UJ, Scherer PE. 2013. Selective inhibition of hypoxia-inducible factor 1α ameliorates adipose tissue dysfunction. Mol Cell Biol 33:904–917. https://doi.org/10.1128/MCB.00951-12.
15. Henegar C, Tordjman J, Achard V, Lacasa D, Cremer I, Guerre-Millo M, Poitou C, Basdevant A, Stich V, Viguerie N, Langin D, Bedossa P, Zucker JD, Clement K. 2008. Adipose tissue transcriptomic signature highlights the pathological relevance of extracellular matrix in human obesity. Genome Biol 9:R14. https://doi.org/10.1186/gb-2008-9-1-r14.
16. Divoux A, Tordjman J, Lacasa D, Veyrie N, Hugol D, Aissat A, Basdevant A, Guerre-Millo M, Poitou C, Zucker J-D, Bedossa P, Clément K. 2010. Fibrosis in human adipose tissue: composition, distribution, and link with lipid metabolism and fat mass loss. Diabetes 59:2817–2825. https://doi.org/10.2337/db10-0585.
17. Spencer M, Unal R, Zhu B, Rasouli N, McGehee RE, Jr, Peterson CA, Kern PA. 2011. Adipose tissue extracellular matrix and vascular abnormalities in obesity and insulin resistance. J Clin Endocrinol Metab 96:E1990–E1998. https://doi.org/10.1210/jc.2011-1567.
18. Sun K, Tordjman J, Clement K, Scherer PE. 2013. Fibrosis and adipose tissue dysfunction. Cell Metab 18:470–477. https://doi.org/10.1016/j.cmet.2013.06.016.
19. Khan T, Muise ES, Iyengar P, Wang ZV, Chandalia M, Abate N, Zhang BB, Bonaldo P, Chua S, Scherer PE. 2009. Metabolic dysregulation and adipose tissue fibrosis: role of collagen VI. Mol Cell Biol 29:1575–1591. https://doi.org/10.1128/MCB.01300-08.
20. Park J, Scherer PE. 2012. Adipocyte-derived endotrophin promotes malignant tumor progression. J Clin Invest 122:4243–4256. https://doi.org/10.1172/JCI63930.
21. Lee YS, Kim JW, Osborne O, Oh DY, Sasik R, Schenk S, Chen A, Chung H, Murphy A, Watkins SM, Quehenberger O, Johnson RS, Olefsky JM. 2014. Increased adipocyte O_2 consumption triggers HIF-1α, causing inflammation and insulin resistance in obesity. Cell 157:1339–1352. https://doi.org/10.1016/j.cell.2014.05.012.
22. Cinti S, Mitchell G, Barbatelli G, Murano I, Ceresi E, Faloia E, Wang S, Fortier M, Greenberg AS, Obin MS. 2005. Adipocyte death defines macrophage localization and function in adipose tissue of obese mice and humans. J Lipid Res 46:2347–2355. https://doi.org/10.1194/jlr.M500294-JLR200.
23. Divoux A, Moutel S, Poitou C, Lacasa D, Veyrie N, Aissat A, Arock M, Guerre-Millo M, Clément K. 2012. Mast cells in human adipose tissue: link with morbid obesity, inflammatory status, and diabetes. J Clin Endocrinol Metab 97:E1677–E1685. https://doi.org/10.1210/jc.2012-1532.
24. Gregor MF, Hotamisligil GS. 2011. Inflammatory mechanisms in obesity. Annu Rev Immunol 29:415–445. https://doi.org/10.1146/annurev-immunol-031210-101322.
25. Kim M, Neinast MD, Frank AP, Sun K, Park J, Zehr JA, Vishvanath L, Morselli E, Amelotte M, Palmer BF, Gupta RK, Scherer PE, Clegg DJ. 2014. ERα upregulates Phd3 to ameliorate HIF-1 induced fibrosis and inflammation in adipose tissue. Mol Metab 3:642–651. https://doi.org/10.1016/j.molmet.2014.05.007.
26. Unger RH, Clark GO, Scherer PE, Orci L. 2010. Lipid homeostasis, lipotoxicity, and the metabolic syndrome. Biochim Biophys Acta 1801:209–214. https://doi.org/10.1016/j.bbalip.2009.10.006.
27. Kusminski CM, Shetty S, Orci L, Unger RH, Scherer PE. 2009. Diabetes and apoptosis: lipotoxicity. Apoptosis 14:1484–1495. https://doi.org/10.1007/s10495-009-0352-8.
28. Rosen ED, Spiegelman BM. 2014. What we talk about when we talk about fat. Cell 156:20–44. https://doi.org/10.1016/j.cell.2013.12.012.
29. Savage DB, Petersen KF, Shulman GI. 2007. Disordered lipid metabolism and the pathogenesis of insulin resistance. Physiol Rev 87:507–520. https://doi.org/10.1152/physrev.00024.2006.
30. Iyengar P, Espina V, Williams TW, Lin Y, Berry D, Jelicks LA, Lee H, Temple K, Graves R, Pollard J, Chopra N, Russell RG, Sasisekharan R, Trock BJ, Lippman M, Calvert VS, Petricoin EF, III, Liotta L, Dadachova E, Pestell RG, Lisanti MP, Bonaldo P, Scherer PE. 2005. Adipocyte-derived collagen VI affects early mammary tumor progression *in vivo*, demonstrating a critical interaction in the tumor/stroma microenvironment. J Clin Invest 115:1163–1176. https://doi.org/10.1172/JCI23424.
31. Pasarica M, Gowronska-Kozak B, Burk D, Remedios I, Hymel D, Gimble J, Ravussin E, Bray GA, Smith SR. 2009. Adipose tissue collagen VI in obesity. J Clin Endocrinol Metab 94:5155–5162. https://doi.org/10.1210/jc.2009-0947.
32. Aigner T, Hambach L, Söder S, Schlötzer-Schrehardt U, Pöschl E. 2002. The C5 domain of Col6A3 is cleaved off from the Col6 fibrils immediately after secretion. Biochem Biophys Res Commun 290:743–748. https://doi.org/10.1006/bbrc.2001.6227.
33. Lamande SR, Morgelin M, Adams NE, Selan C, Allen JM. 2006. The C5 domain of the collagen VI α3(VI) chain is critical for extracellular microfibril formation and is present in the extracellular matrix of cultured cells. J Biol Chem 281:16607–16614. https://doi.org/10.1074/jbc.M510192200.
34. Eruzun H, Toprak ID, Arman Y, Yilmaz U, Ozcan M, Kutlu Y, Irmak S, Kutlu O, Yoldemir SA, Altun O, Cil EO, Tukek T. 2019. Serum endotrophin levels in patients with heart failure with reduced and mid-range ejection fraction. Eur J Intern Med 64:29–32. https://doi.org/10.1016/j.ejim.2019.04.016.
35. Rasmussen DGK, Fenton A, Jesky M, Ferro C, Boor P, Tepel M, Karsdal MA, Genovese F, Cockwell P. 2017. Urinary endotrophin predicts disease progression in patients with chronic kidney disease. Sci Rep 7:17328. https://doi.org/10.1038/s41598-017-17470-3.
36. Fenton A, Jesky MD, Ferro CJ, Sorensen J, Karsdal MA, Cockwell P, Genovese F. 2017. Serum endotrophin, a type VI collagen cleavage product, is associated with increased mortality in chronic kidney disease. PLoS One 12:e0175200. https://doi.org/10.1371/journal.pone.0175200.
37. Sun K, Park J, Gupta OT, Holland WL, Auerbach P, Zhang N, Goncalves Marangoni R, Nicoloro SM, Czech MP, Varga J, Ploug T, An Z, Scherer PE. 2014. Endotrophin triggers adipose tissue fibrosis and metabolic dysfunction. Nat Commun 5:3485. https://doi.org/10.1038/ncomms4485.
38. Funcke JB, Scherer PE. 2019. Beyond adiponectin and leptin: adipose tissue-derived mediators of inter-organ communication. J Lipid Res 60:1648–1684. https://doi.org/10.1194/jlr.R094060.
39. Bu D, Crewe C, Kusminski CM, Gordillo R, Ghaben AL, Kim M, Park J, Deng H, Xiong W, Liu XZ, Lonning PE, Halberg N, Rios A, Chang Y, Gonzalez A, Zhang N, An Z, Scherer PE. 2019. Human endotrophin as a driver of malignant tumor growth. JCI Insight 5:125094. https://doi.org/10.1172/jci.insight.125094.
40. Lee C, Kim M, Lee JH, Oh J, Shin HH, Lee SM, Scherer PE, Kwon HM, Choi JH, Park J. 2019. COL6A3-derived endotrophin links reciprocal interactions among hepatic cells in the pathology of chronic liver disease. J Pathol 247:99–109. https://doi.org/10.1002/path.5172.
41. Thrailkill KM, Clay Bunn R, Fowlkes JL. 2009. Matrix metalloproteinases: their potential role in the pathogenesis of diabetic nephropathy. Endocrine 35:1–10. https://doi.org/10.1007/s12020-008-9114-6.
42. Nagase H, Visse R, Murphy G. 2006. Structure and function of matrix metalloproteinases and TIMPs. Cardiovasc Res 69:562–573. https://doi.org/10.1016/j.cardiores.2005.12.002.
43. Itoh Y. 2006. MT1-MMP: a key regulator of cell migration in tissue. IUBMB Life 58:589–596. https://doi.org/10.1080/15216540600962818.
44. Sternlicht MD, Werb Z. 2001. How matrix metalloproteinases regulate cell behavior. Annu Rev Cell Dev Biol 17:463–516. https://doi.org/10.1146/annurev.cellbio.17.1.463.
45. McCawley LJ, Matrisian LM. 2001. Matrix metalloproteinases: they're not just for matrix anymore!. Curr Opin Cell Biol 13:534–540. https://doi.org/10.1016/S0955-0674(00)00248-9.
46. Zucker S, Pei D, Cao J, Lopez-Otin C. 2003. Membrane type-matrix metalloproteinases (MT-MMP). Curr Top Dev Biol 54:1–74. https://doi.org/10.1016/s0070-2153(03)54004-2.
47. Lin D, Chun T-H, Kang L. 2016. Adipose extracellular matrix remodelling in obesity and insulin resistance. Biochem Pharmacol 119:8–16. https://doi.org/10.1016/j.bcp.2016.05.005.
48. Chavey C, Mari B, Monthouel MN, Bonnafous S, Anglard P, Van Obberghen E, Tartare-Deckert S. 2003. Matrix metalloproteinases are differentially expressed in adipose tissue during obesity and modulate adipocyte differentiation. J Biol Chem 278:11888–11896. https://doi.org/10.1074/jbc.M209196200.
49. Chun TH, Hotary KB, Sabeh F, Saltiel AR, Allen ED, Weiss SJ. 2006. A pericellular collagenase directs the three-dimensional development of white adipose tissue. Cell 125:577–591. https://doi.org/10.1016/j.cell.2006.02.050.
50. Chun TH, Inoue M, Morisaki H, Yamanaka I, Miyamoto Y, Okamura T, Sato-Kusubata K, Weiss SJ. 2010. Genetic link between obesity and MMP14-dependent adipogenic collagen turnover. Diabetes 59:2484–2494. https://doi.org/10.2337/db10-0073.
51. Welsh S, Williams R, Kirkpatrick L, Paine-Murrieta G, Powis G. 2004. Antitumor activity and pharmacodynamic properties of PX-478, an inhibitor of hypoxia-inducible factor-1α. Mol Cancer Ther 3:233–244.
52. Koh MY, Spivak-Kroizman T, Venturini S, Welsh S, Williams RR, Kirkpatrick DL, Powis G. 2008. Molecular mechanisms for the activity of PX-478, an

antitumor inhibitor of the hypoxia-inducible factor-1alpha. Mol Cancer Ther 7:90–100. https://doi.org/10.1158/1535-7163.MCT-07-0463.
53. Zhu Y, Zang Y, Zhao F, Li Z, Zhang J, Fang L, Li M, Xing L, Xu Z, Yu J. 2017. Inhibition of HIF-1α by PX-478 suppresses tumor growth of esophageal squamous cell cancer *in vitro* and *in vivo*. Am J Cancer Res 7:1198–1212.
54. Lengyel E, Makowski L, DiGiovanni J, Kolonin MG. 2018. Cancer as a matter of fat: the crosstalk between adipose tissue and tumors. Trends Cancer 4:374–384. https://doi.org/10.1016/j.trecan.2018.03.004.
55. Mariman EC, Wang P. 2010. Adipocyte extracellular matrix composition, dynamics and role in obesity. Cell Mol Life Sci 67:1277–1292. https://doi.org/10.1007/s00018-010-0263-4.
56. Zhao Y, Gu X, Zhang N, Kolonin MG, An Z, Sun K. 2016. Divergent functions of endotrophin on different cell populations in adipose tissue. Am J Physiol Endocrinol Metab 311:E952–E963. https://doi.org/10.1152/ajpendo.00314.2016.
57. Heumuller SE, Talantikite M, Napoli M, Armengaud J, Morgelin M, Hartmann U, Sengle G, Paulsson M, Moali C, Wagener R. 2019. C-terminal proteolysis of the collagen VI α3 chain by BMP-1 and proprotein convertase(s) releases endotrophin in fragments of different sizes. J Biol Chem 294:13769–13780. https://doi.org/10.1074/jbc.RA119.008641.
58. Sun K, Kusminski CM, Luby-Phelps K, Spurgin SB, An YA, Wang QA, Holland WL, Scherer PE. 2014. Brown adipose tissue derived VEGF-A modulates cold tolerance and energy expenditure. Mol Metab 3:474–483. https://doi.org/10.1016/j.molmet.2014.03.010.
59. Sung HK, Doh KO, Son JE, Park JG, Bae Y, Choi S, Nelson SM, Cowling R, Nagy K, Michael IP, Koh GY, Adamson SL, Pawson T, Nagy A. 2013. Adipose vascular endothelial growth factor regulates metabolic homeostasis through angiogenesis. Cell Metab 17:61–72. https://doi.org/10.1016/j.cmet.2012.12.010.
60. Nam DH, Rodriguez C, Remacle AG, Strongin AY, Ge X. 2016. Active-site MMP-selective antibody inhibitors discovered from convex paratope synthetic libraries. Proc Natl Acad Sci U S A 113:14970–14975. https://doi.org/10.1073/pnas.1609375114.
61. He A, Shen X, Ma Q, Cao J, von Gise A, Zhou P, Wang G, Marquez VE, Orkin SH, Pu WT. 2012. PRC2 directly methylates GATA4 and represses its transcriptional activity. Genes Dev 26:37–42. https://doi.org/10.1101/gad.173930.111.
62. Zhao Y, Li X, Yang L, Eckel-Mahan K, Tong Q, Gu X, Kolonin MG, Sun K. 2018. Transient overexpression of VEGF-A in adipose tissue promotes energy expenditure via activation of the sympathetic nervous system. Mol Cell Biol 38:e00242-18. https://doi.org/10.1128/MCB.00242-18.
63. Yang L, Li X, Tang H, Gao Z, Zhang K, Sun K. 2019. A unique role of carboxylesterase 3 (Ces3) in β-adrenergic signaling-stimulated thermogenesis Diabetes 68:1178–1196. https://doi.org/10.2337/db18-1210.